RSC Advances

ROYAL SOCIETY OF CHEMISTRY

www.rsc.org/advances

DFT/TDDFT insights into the chemistry, biochemistry and photophysics of copper coordination compounds

Athanassios C. Tsipis

DOI: 10.1039/b000000x [DO NOT ALTER/DELETE THIS TEXT]

In this review the recent progress in DFT/TDDFT application to copper coordination compounds is highlighted. Selected most recent applications that best illustrate the promise of DFT in the following active areas of copper coordination chemistry: (i) mechanistic studies of copper-catalyzed reactions, (ii) investigating the nature of bonding in copper coordination compounds, (iii) the bioactivity and biochemistry of copper coordination compounds and (iv) the photophysics (absorption and emission spectra) of copper coordination compounds are reviewed. This review is intended to be of interest to both experimentalists and theorists in the expanded field of copper coordination chemistry.

1 Introduction

Copper forms a variety of coordination compounds in both of the two common relatively stable oxidation states, 1+ and 2+. However, in many organometallic reactions involving copper, the reaction mechanism invokes a copper intermediate with oxidation state 3+, but Cu(III) compounds are rare in chemistry in general and until recently organocopper(III) species have been elusive. In 2007 the first spectroscopic evidence was obtained for the involvement of Cu(III) in the conjugate addition of the Gilman reagent, $R_2CuLi{\cdot}LiX$ (X = Cl, Br, I) to an enone.[1] The properties of copper coordination compounds, whether in classical copper complexes, in organocopper compounds, or in bioinorganic model compounds are largely determined by the nature of ligands and donor atoms bound to the metal ion.[2,3] In that context copper compounds have found a widespread use in a range of applications in catalysis, medicinal chemistry and applied material sciences relating to electron transport devices and organic light-emitting diodes (OLEDs).

1.1. Copper coordination compounds as catalysts

Copper compounds have been widely utilized for over a century, mainly in the construction of carbon-carbon and carbon heteroatom bonds.[4,5] They have been used also as catalysts in a wide range of catalytic reactions, such as the oxidative alkane dehydrogenation,[6-8] the Sonogashira–Hagihara-type reactions,[9,10] the homocoupling of terminal alkynes to 1,3-diynes,[11,12] the direct C–H bond activation,[13-21] C-C bond cleavage reactions,[22-24] and a variety of copper-catalyzed cyclization reactions,[25-33] Very recently, a general overview of chiral bimetallic cuprates widely used in copper-catalyzed asymmetric synthesis was presented by Woodward.[34] Nowadays, the generation of more efficient and selective, eco-friendly, copper-based catalysts for applications with industrial relevance has triggered the interest of inorganic chemists. Copper complexes are also used to mimic the active site of type-3 copper

proteins such as hemocyanin, an oxygen-transport protein, tyrosinase and catechol oxidase that use dioxygen to catalyze the oxidation of phenols and *o*-diphenols to *o*-quinones, respectively.[35,36]

1.2. Bioactive copper coordination compounds

Copper is an essential trace element common in all living organisms. It is present as a cofactor in several metalloproteins with enzymatic functions: its unique redox chemistry, based on the easily reversible redox couple Cu(II)/Cu(I), is crucial for several biochemical processes.[37] Copper is also found in several enzymes, such as cytochrome oxidase and ascorbate oxidase, and is also present in superoxide dismutase (SOD), the biochemical role of which, as the name implies, is to catalyze the dismutation of superoxide ions. Although copper has a long history of medical application, coordination compounds of Cu(I) and Cu(II) have been investigated as potential antiproliferative agents only in the last few decades, particularly after the discovery of cisplatin, the most widely used anticancer metallodrug. Up to now, a great variety of copper complexes have been tested as cytotoxic agents and found to be endowed with an antitumor activity in several *in vitro* tests and few *in vivo* experiments.[38,39] An overview of the multiple bioactivity of copper complexes and their applications in medicine as potential drugs for therapeutic intervention in various diseases has recently been reported.[40] The copper-based cytotoxic drugs show a wide range of diverse pharmacodynamics and possibly diverse mechanisms lie behind their cytotoxicity. The current goal for the inorganic investigators is now to design and produce novel copper-based anticancer drugs to improve clinical effectiveness, to reduce general toxicity, and to broaden the spectrum of activity.[41]

1.3. Photophysics of copper coordination compounds

Luminescent copper(I) complexes are currently receiving much attention due to their potential applications in various fields, such as organic light-emitting diodes (OLEDs),[42,43] light-emitting electrochemical cells (LECs),[44] supramolecular assemblies,[45] chemical sensors,[46] solar-energy conversion schemes,[47] dye sensitized solar cells,[48] biological probing and oxygen sensing.[49,50] They are being environmentally friendly, less expensive, exhibiting intriguing coordination modes, rich photochemical and photophysical properties. Many of these complexes have been reported to be luminescent and their emission behaviour varies with structures/steric effects of the coordinated ligands. OLED is a rapidly emerging technology in the flat panel display industry, with many advantages over liquid crystal (LCD) or plasma displays, generating their own light and do not require backlighting. These features make them attractive for use in hand held devices such as cell phones, digital cameras, and portable video games in addition to computer monitors and full-sized televisions.[51]

A large number of luminescent Cu(I) complexes are known. These complexes can be generally divided into the following classes: cuprous halide clusters,[52] chalcogenide clusters,[53] acetylide clusters,[53] trinuclear pyrazolate complexes,[54-56] and mononuclear Cu(I) complexes most commonly coordinated by two N^N ligands (N^N = diimine), or an N^N and one P^P ligand (P^P = diphosphane).[57-60] Each is characterized by its unique photophysical properties with excited states varying from cluster-centered (CC), metal-to-ligand charge transfer (MLCT), ligand-to-metal charge transfer (LMCT), ligand-to-ligand charge transfer (LLCT), or ligand-centered

(LC). LLCT and LC excitations were observed in a series of three-coordinate copper(I) diarylamidophosphane complexes that combine efficient photoluminescence in fluid solution at room temperature, with quantum yields ranging from 0.11 to 0.24.[61] Three-coordinated Cu(I) complexes bearing bulky N-heterocyclic carbene ligands and anionic pyridyl-benzimidazole gave moderate solution emission and efficient solid state emission.[62] Four-coordinate Cu(I) complexes with anionic benzimidazole-based ligands have also been reported.[63] Very recently Lazorski and Castellano[64] reported a concise overview of the most recent and most influential advances in the photophysical properties of $Cu(I)(L)_2$ and Cu(I)LP complexes (where L = substituted polypyridyl ligands and P = phosphane based ligand such as bis[(2-diphenylphosphino)phenyl]-ether (DPEphos) or triarylphosphane (PAr_3)) in fluid solution and select applications in solar energy conversion technologies and light-emitting devices.

2 DFT/TDDFT insights on copper coordination chemistry

Density functional theory (DFT) and time-dependent DFT (TDDFT) have nowadays become general tools to the understanding and predicting the behavior of a broad range of chemical, physical, and biological phenomena featuring the realm of coordination chemistry. DFT describes the electronic states of atoms and molecules in terms of the three-dimentional electron density, which is a great simplification over the wave function theory (WFT) which is based on the 3*N*-dimentional antisymmetric wave function for a system with *N* electrons. Such simplification rendered DFT the preferred method for electronic structure theory for complex chemical systems. DFT competes well in accuracy with the correlated WFT methods, but with much lower computational cost. These advantages of DFT are still greater for metals, especially transition metals.[65] An overview of recent progress in DFT/TDDFT applications to coordination chemistry providing selected applications in a number of very active areas of coordination chemistry, such as bonding, catalysis and spectroscopy was reported recently.[66] Emphasis was given on the practical aspects that may be interesting for experimentalists wishing to employ DFT/TDDFT alongside to their experimental work and outlined some general instructions of how to select the proper DFT computational protocol for a particular study. Timely exhaustive assessment of DFT methods applied in transition metal chemistry has been reviewed by Cramer and Truhlar.[65] Frank Neese[67] provided a detailed account of DFT and its application to the calculation of molecular properties of inorganic compounds. A very recent publication in *Coordination Chemistry Reviews* by Kepp[68], offering a discussion of the physical effects and ingredients in functionals, their systematic errors and approaches to deal with them, in order to identify broadly applicable methods for inorganic chemistry is commended to the readers and researchers in the field of copper coordination chemistry.

2.1. Structural and optical benchmarking of copper coordination compounds

The number of papers reporting DFT calculations on copper coordination compounds has recently increased covering a wide research area providing insights into the structures and electronic states of copper coordination compounds, the mechanisms of organocopper catalyzed reactions, the electronic (absorption and

emission) and vibrational spectra. Given this wide remit, it is our wish to comment here on the more recent developments in the area, presenting a few case examples of successful applications of DFT methods in the coordination chemistry of copper. At this point it should be stressed that DFT and TDDFT calculations on copper coordination compounds have to be validated by rigorous *ab initio* or by accurate experimental data for each new problem or new system, particularly when investigating excited states. This is due to the fact that at the present time, no universally and transferable selection of density functionals (DFs) can be employed, rendering the choice of DFT computational protocols, highly influenced by the problem at hand and the most popular ones in the literature have been derived by careful comparison with experiment.

A thorough study of various computational protocols (DF/basis set combinations) was carried out for the description of relevant Cu(I) and Cu(II) centres in reasonable sized systems, with properties closer to systems that are present in copper coordination spheres of general interest.[69] The performance of a total of 18 DFs and 14 different basis sets in the determination of geometrical properties of an enlarged dataset of 50 copper complexes (24 of Cu(I) and 26 of Cu(II)) was evaluated. In general, the more sophisticate the DFT method, better is the geometrical description of the copper complexes. In particular, double hybrid-generalized gradient approximation (DH-GGA) and long range corrected-hybrid-GGA (LC-H-GGA) DFs provide the best geometrical description of the systems. The hybrid-meta-GGA (HM-GGA) M06 DF gave also identical performances, surpassing the most popular B3LYP hybrid-GGA (H-GGA). Other DFs, such as the PBE pure-GGA or the M06L meta-GGA also conveyed promising results. Dispersion corrections, namely DFT-D and DFT-D3, have not granted increased performances in the dataset considered, possibly due to the smaller sizes of the tested complexes. It was shown that there are several competitive alternatives for the determination of metal-ligand bond-lengths and angles in copper complexes, but still, there is no universally best behaving computational protocol for the description of the geometry of copper complexes; and so, the reader should tread carefully through the choices of methodologies for embarking on future studies of copper complexes.[69]

More recently, Herres-Pawlis and co-workers[70] reported a comprehensive computational benchmarking of the structural and optical properties of a bis(chelate) copper(I) guanidine–quinoline complex. The geometric benchmarking recommends the BP86/6-311G(d) computational protocol for best accordance of gas-phase calculations to the solid state structures from X-ray measurements whereas the optical benchmarking gives best resemblance to experimental spectra when applying the B3LYP/def2-TZVP computational protocol.

The coordination number of various experimentally known Cu(I) coordination compounds with thiophenolato ligands has been studied using PBE0, a hybrid GGA functional, and a variety of all-electron basis sets and basis set-RECP combinations, including several commonly used ones.[71] Addition of dispersion corrections improves the results both qualitatively and quantitatively. Energy decomposition analysis (EDA) revealed that two opposing contributions play a major role: a stabilizing contribution due to the interaction energy of the added ligand, which leads to higher coordination numbers and a destabilizing contribution due to the deformation energy of the copper's coordination sphere prior to the ligand addition, which favors lower coordination numbers. Generally, ligands that form tricoordinate complexes had consistently higher interaction energies and lower deformation

energies than those forming two-coordinate Cu(I) complexes.

It is suggested the new comer to the field of computational chemistry to run some "calibration" calculations on some model molecules similar to the ones he/she wants to study where he/she can compare the accuracy of possible DFs and basis sets to decide which combination is best for his/her "production" calculations and validate the calculations by rigorous *ab initio* or by accurate experimental data for each new problem or new system.

2.2. The nature of bonding in copper coordination compounds

2.2.1. Copper(I) complexes. Weak attraction between transition metal atoms with closed shell electron configuration, such as Cu(I), Ag(I) and Au(I), was first evidenced by Schmidbaur *et al*. in the cases of intra- and intermolecular Au(I)···Au(I) contacts.[72,73] The term 'aurophilicity' has been coined to describe this special kind of metal–metal bonding interaction,[73] which can be as strong as 11 kcal/mol.[74] These closed-shell interactions in inorganic chemistry have been reviewed by Pyykkö.[75] The occurrence of Cu(I)···Cu(I) metallophilic effects (the so called cuprophilicity) has been the subject of a long debate due to the intramolecular character of the reported interactions. Metallophilic interactions are not easy to characterize from quantum chemical calculations. In particular cuprophilicity is relatively weak, and is easily confused by other intermolecular interactions such as hydrogen bonds or $\pi\cdots\pi$ interactions. Therefore, a theoretical basis for the nature of the Cu(I)···Cu(I) d^{10}-d^{10} interactions has been continuously evolving.

Recently, Dinda and Samuelson[76] employing the "atoms in molecules" (AIM) concept developed by Bader[77] threw some light on the nature of Cu(I)···Cu(I) interactions. AIM analysis revealed that a bond critical point (BCP) between two Cu atoms is present in most cases of copper(I) complexes considered and points to the presence of an attractive metallophilic interaction similar to other well-documented weak interactions. Noteworthy the nature of the BCP in terms of the electron density, ρ, and its Laplacian, $\nabla^2\rho$, is quite similar to the nature of critical points observed in hydrogen bonds in the same systems.

A new class of cyclic copper(I) hydrides (hydrocoppers), Cu_nH_n (n = 3-6) as the cyclic hydrocarbon analogues in the diverse tapestry of inorganic chemistry, introducing, for the first time, the concept of d orbital aromaticity was reported in 2003.[78] DFT calculations at the B3LYP/6-311+G(d,p) level predicted that the Cu_nH_n hydrocoppers are stable molecules with a perfect planar configuration. The planarity and structural integrity of the cyclic Cu_nH_n molecules was accounted for by the bonding mechanism characterizing the all metallacycle rings that involves σ-, and highly delocalized π- and δ-type MOs, resulting from the bonding interaction of the 3d AOs of the ring Cu(I) atoms, which support a ring current, thus rendering hydrocoppers aromatic molecules. The estimated molecular electrostatic potential (MEP) of the cyclic Cu_nH_n molecules, being positive over the all-metal rings and negative on the hydride ligands, strongly supports electrophilic substitution reactions, which are characteristic of the aromatic systems. The aromaticity/antiaromaticity of the cyclic hydrocoppers was also quantified by the magnetic criterion, *viz*. nucleus-independent chemical shift (NICS) proposed by Schleyer.[79]

Li et al.,[80,81] stimulated by the proposal of aromatic Cu_4H_4 and Cu_5H_5 hydrocoppers, presented the first theoretical evidence for tetracoordinate and

pentacoordinate planar non-metal atoms X (X = B, C, N, O) hosted at the center of the four- and five-member hydrocopper rings. Natural bond orbital (NBO) population analyses provided insights into the atomic charge distribution and electron configurations of the Cu_nH_nX (n = 4, 5; X = B, C, N, O) molecules indicating considerable electron transfer from the Cu ring atoms to the more electronegative X center. Accordingly, the X atoms serve as the negatively charged nonmetal centers, the Cu atoms at the periphery form a positively charged ring, and the bridging H atoms carry negative charges to maintain the overall charge balance.

The structural, energetic, magnetotropic, and spectroscopic properties of the aromatic coinage metalated benzenes with the general formulae 1,3,5-$C_6H_3M_3$ and C_6M_6 (M = Cu, Ag, Au) were analyzed at the PBE0/Def2-QZVPP level of theory and compared to the respective properties of the unsubstituted archetype aromatic benzene molecule.[82] The aromatic coinage metalated benzenes exhibit unique properties which are of interest for potential application in several technological issues. Furthermore these findings expand the aromaticity concept to dual-ring systems involving two orthogonal delocalization channels.

The molecular and electronic structures, bonding features, magnetotropicity and absorption spectra of benzene−trinuclear Cu(I) and Ag(I) trihalide columnar binary stacks with the general formula $[c\text{-}M_3(\mu_2\text{-}X)_3]_n(C_6H_6)_m$ (M = Cu, Ag; X = halide; n, m ≤ 2) have been investigated by means of electronic structure calculation methods at the B97D/Def2-TZVP level of theory.[83] In all binary stacks the plane of the alternating $c\text{-}M_3(\mu_2\text{-}X)_3$ and benzene decks adopts an almost parallel orientation. Energy decomposition analysis (EDA) revealed that the dominant term that characterizes the $[c\text{-}M_3(\mu_2\text{-}X)_3]\cdots(C_6H_6)$ interactions arises primarily from dispersion and electrostatic forces while the covalent interactions are predicted to be negligible. Charge decomposition analysis (CDA) illustrated very small charge transfer from C_6H_6 toward the $[c\text{-}M_3(\mu_2\text{-}X)_3]$ clusters, thus reflecting weak π-base/π-acid interactions. The good linear correlation between ΔE_{disp} and the calculated polarizability α of the binary stacks indicated that polarizability is the determining factor of dispersion interactions (Fig. 1).

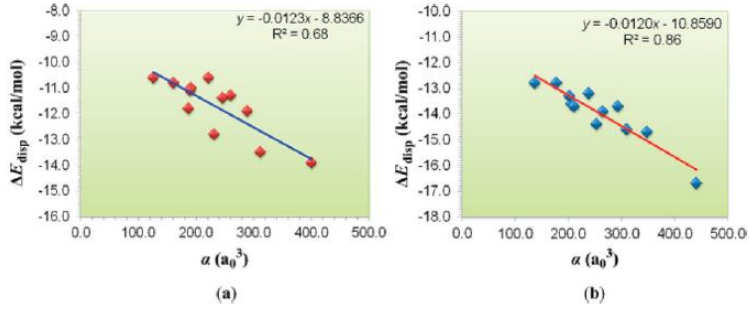

Fig. 1 Linear correlations of the dispersion energy term, ΔE_{disp}, versus the mean isotropic polarizability, α, for the $[c\text{-}Cu_3(\mu_2\text{-}X)_3]_n(C_6H_6)_m$ (**a**) and $[c\text{-}Ag_3(\mu_2\text{-}X)_3]_n(C_6H_6)_m$ (**b**) binary stacks computed at the B97D/Def2-TZVP level (reproduced with permission from ref. 83).

The magnetotropicity of the binary stacks evaluated by the $NICS_{zz}$-scan curves indicated an enhancement of the diatropicity (magnetic aromaticity) of the triangular metal ring upon interaction with the aromatic benzene molecule. The interacting

rings keep their magnetic response properties in the clusters, but showing an appreciable enhancement of the diatropic (aromatic) character due to the superposition (coupling) of the diamagnetic ring currents of the inorganic and benzene rings.

A systematic and comparative study using CCSD and DFT (employing the hybrid B3LYP, B3PW91, PBE0, and w-B97X non local GGAs, the Minnessotta M06 and M06-L, the local meta-GGA TPSS and the non-local hybrid TPSSh, DSD-PBEP86, and local BP86 and PBE DFs) computational approaches was performed to investigate the electronic structure, chemical bonding, and absorption spectra of $[CuE]^{+/0/-}$ (E = C, Si, Ge, Sn, Pb) diatomics.[84] Among the tested methods, DSDPBEP86, M06, B3PW91, B3LYP, and PBE0 were found, in terms of chemical accuracy, error margin and computational expense, to overall perform best for the calculation of spectroscopic constants of the $[CuE]^{+/0/-}$ diatomics. The DSD-PBEP86 DF performs equally well as the high quality C-RCCSD(T)+DKH2 and MRCI+DKH2+Q *ab initio* approaches in the calculation of the spectroscopic constants of the CuC molecule and provides accurate spectroscopic constants for the $[CuE]^{+/0/-}$ diatomics. Acceptably reliable spectroscopic constants were also obtained at the B3LYP, B3PW91, PBE0, M06, M06L, and TPSS levels, whereas the worst results are obtained at the CCSD level. The Wiberg Bond Orders of the Cu-E bonds estimated by means of NBO analysis method indicate formation of a single (two electron) σ-bond in all the neutral CuE diadomics, except of the CuC ($^4\Sigma^-$) and $[CuC]^+$ ($^3\Sigma^+$) diatomics, where a half (one electron) σ-bond is formed. All the remaining $[CuE]^{+/0/-}$ species involve formation of a single (two electron) σ-bond. The spatial organization of the bonding between Cu and E atoms in the $[CuE]^{+/0/-}$ molecules can easily be recognized by arrangement of the monosynaptic and disynaptic basins in the cut-plane electron localization function (ELF) representations (Fig. 2).

The molecular structure and properties of five Cu(I) complexes with the general formula $[CuL_2]^+$ (L = bipyridine ligands) proposed as sensitizers in dye-sensitized solar cells have been studied by DFT methods employing the M06 HM-GGA density functional and the LANL2DZ and DZVP basis sets.[85] The characterization of the molecular systems included the calculation of geometric parameters, ultraviolet-visible spectra, electronic excited states, molecular orbitals, and chemical reactivity parameters.

Geometries, bonding nature, and electronic structures of model (N^N)Cu(O_2) (N^N = β-diketiminate) complexes were investigated by DFT and multistate restricted active space multiconfigurational second-order perturbation (MS-RASPT2) methods.[86] The model $(N^N)_mCu(O_2)$ (N^N = PhNC(Me)CHC(Me)NPh) complexes adopting a structure with C_{2v} symmetry exhibit significant superoxo (O_2^-) character as it is found from the occupation numbers of natural orbitals and the O−O π bond order ($BO_{O\text{-}O}$), which is independent of the number of d electrons and the oxidation state of metal center.

$$BO_{O\text{-}O} = \frac{q_{\pi_x} + q_{\pi_z} - q_{\pi_x^*} - q_{\pi_z^*}}{2}$$

where $q_{\pi x}$ is the occupation number of the π_x orbital. The π bond order is zero (0) for peroxo and 0.5 for superoxo coordinated O_2 ligand. The O−O bond length is influenced not only by the charge transfer (CT) from (N^N)Cu to O_2 but also by the

CT from O_2 π^* and π to (N^N)Cu. The calculations provided clear and well understanding of the nature of the metal-dioxygen moiety and the interaction between the metal and the dioxygen molecule.

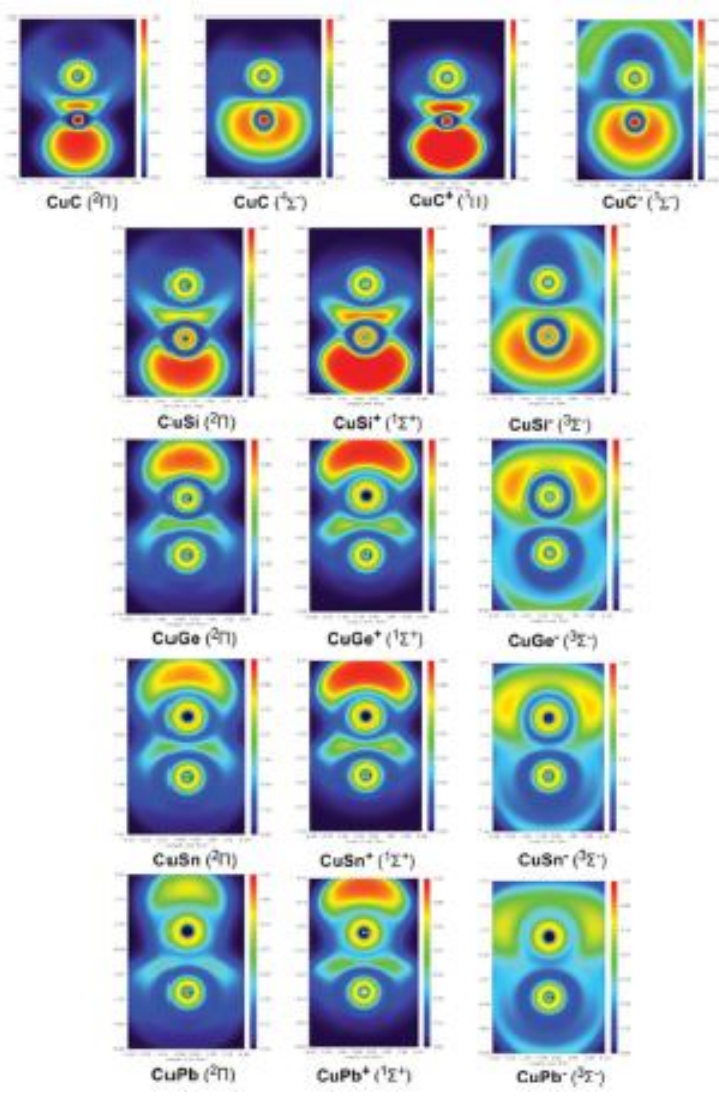

Fig. 2 Cut-plane ELF representation of the $[CuE]^{+/0/-}$ (E = C, Si, Ge, Sn, Pb) diatomics (reproduced with permission from ref. 84).

2.2.2 Copper(II) complexes. A series of Cu(II) and Cu(I) complexes with general formula $[Cu(NH_3)_m(H_2O)_n]^{2+/+}$ (n = 0 to 4 0r 6; m+n = 4 or 6) was investigated by DFT methods at the B3PW91/6-31+G(d) and B3LYP/6-311++G(2*df*,2*pd*) (single point calculations) levels of theory.[87] The most stable Cu(II) and Cu(I) complexes are the four- and two-coordinated structures, respectively. The most stable structures exhibit the shortest Cu–N (1.9/2.05 Å for

Cu(I)/Cu(II) species) and Cu–O bonds (1.87/1.96 Å). Natural Population Analysis (NPA) illustrated the strongest copper coordination covalent interactions with two ligands in Cu(I), and four ligands in Cu(II) systems by the most pronounced electron density redistribution. The energy and wave function analyses also confirm copper–ammine bonding to be preferred over copper-aqua one, thereby mixed water/ammonia complexes always prefer to form structures with the NH_3 molecules in the first hydration shell. EDA calculations enlightened the role of Coulomb, exchange repulsion and polarization terms of the metal-ligand interactions at the Hartree-Fock level of theory.

DFT calculations (B3LYP/DZVP) were performed to decipher the bonding of the trihalide ligands in a series of homo and hetero-trihalide Cu(II) Schiff base complexes formulated as [Cu(RdienR)(X)(XY_2)] (RdienR = Schiff base; R = furan, thiophene or pyrrol; X = Cl or Br; Y = Cl, Br or I).[88] The association of the incoming Y_2 halogen molecule with one of the halide X ligands of the precursor [Cu(RdienR)(X_2)] complexes alters their distorted trigonal bipyramidal stereochemistry which is transformed to a distorted square pyramidal geometry. NBO population analysis indicated that the association of the incoming halogen Y_2 molecule with a halide X(1) ligand of the precursor complexes corresponds to donor–acceptor hyperconjugative interactions involving a nonbonding molecular orbital localized on the coordinated X(1) halide ligand, n(X), (donor orbital) and an antibonding molecular orbital localized on the Y_2 molecule, σ^*(Y–Y) (acceptor orbital). The n(X) → r*(Y–Y) donor–acceptor interactions are associated with a second order perturbation stabilization energy, $\Delta E(2)$ of 34.5–52.5 kcal/mol. The loose association of the halogen molecules with the coordinated halide ligand renders the [Cu(RdienR)(X)(XY_2)] complexes good halogen carrier molecules. Charge Decomposition Analysis (CDA) calculations revealed that the charge transferred from the halide ligand to the halogen molecule in the [Cu(RdienR)(X)(XY_2)] complexes follows the trend: Cl → I_2 > Br → I_2 > Cl → Br_2 > Br → Br_2, in line with the trend followed by the occupation of the n(X) donor orbital of the complexes. The estimated interaction energies between the precursor and the halogen molecules amounting to -16.2up to -20.0 kcal/mol illustrated that these interactions are much weaker than the donor–acceptor interactions in the ''free'' $[XY_2]^-$ anions (interaction energies found in the range of -44.9 to -49.2 kcal/mol).

Theoretical calculations based on DFT were performed on both the doublet and quartet states of model trinuclear Cu(II) clusters that have been characterized as *inverse*-9-metallacrown-3 compounds accommodating one or two guest ligands.[89] These trinuclear Cu(II) complexes obtained by reacting Cu(II) salts with PhPyCNO-/X^- "blends" (PhPyCNOH = phenyl 2-pyridyl ketoxime; X^- = OH^-, alkanoato, ClO_4^-) showed a large antiferromagnetic interaction and a discrepancy between the low-temperature magnetic behaviour observed. DFT calculations demonstrated the contribution of both e_g and t_{2g} magnetic orbitals to the magnetic exchange coupling. The latter contribution, although less important, might be due to overlap of the t_{2g} orbitals with the *p*-type orbitals of the central triply bridging oxide ligand, thereby affecting its displacement from the Cu_3 plane and contributing to the antiferromagnetic coupling. The crucial role of the μ_3-O ligand on the antiferromagnetic exchange coupling between the three Cu(II) magnetic centers was evidenced by the excellent linear correlation of the coupling constant *J* with the distance of the μ_3-O ligand from the centroid of the Cu_3 triangle (Fig. 3).

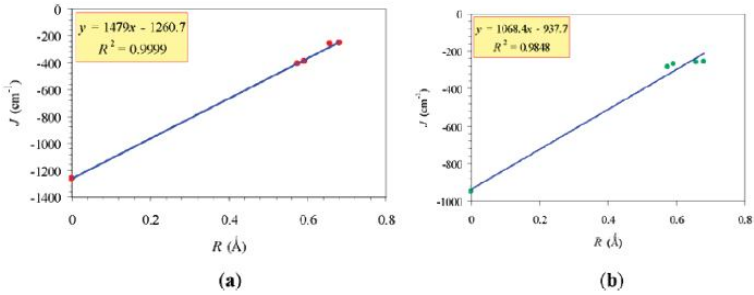

Fig. 3 Linear correlation of the coupling constant *J*, estimated using (**a**) Yamaguchi's model and (**b**) the formula $3|J| = E_{HS} - E_{LS}$, with *R*, the distance of the μ_3-O ligand from the centroid of the Cu_3 triangle (reproduced with permission from ref. 89).

DFT calculations employing the B3LYP functional and the COSMO continuum solvent model were performed to characterize the structure and stability of $[Cu(H_2O)_n]^{2+}$ clusters as a function of coordination number (4, 5, and 6) and cluster size (n = 4−18).[90] The most thermodynamically favored Cu(II) complexes in the gas phase adopt a very open four-coordinate structure formed from a stable square-planar $[Cu(H_2O)_8]^{2+}$ core stabilized by an unpaired electron in the $d_{x^2-y^2}$ orbital of Cu(II). In the aqueous phase, the more compact five-coordinate square-pyramidal geometry is more stable than either the four-coordinate or six-coordinate clusters. The same computational protocol was employed to study the geometric structure, relative energies, and thermodynamic stability of various hydrated Cu^{2+} complexes, $[Cu(MeNH_2)(H_2O)_{n-1}]^{2+}$ and $[Cu(OH)_x(H_2O)_{n-x}]^{2-x}$ (x = 1-3), as a function of metal-ligand coordination number (4-6) and cluster size (n = 4-8, 18).[91] The most stable complexes with $n \leq 8$ in the aqueous phase have nearly square-planar four-coordinate geometry. The exception is $[Cu(OH)_3(H_2O)]^-$, which is stable only in a three-coordinate arrangement. In the presence of the two hydration shells around Cu^{2+}, however, the five-coordinate square pyramidal geometry was found to be the most favorable for $Cu(MeNH_2)^{2+}$(5, 6) and $Cu(OH)^+$(5, 4, 6), and the four-coordinate geometry to be the most stable for $Cu(OH)^2$(4, 5) and $Cu(OH)_3^-$(4). For an accurate prediction of structural and thermodynamic properties of Cu(II) species in aqueous solution, the explicit solvation of the first and the second shells around Cu^{2+} (n = 18) should be taken into consideration.

In recent years, solvent extraction of copper(II) in ammoniacal solutions has received great interest because a large number of low grade copper oxide ores and wastes have been extracted with ammonia leaching. Recently Hu and co-workers[92] presented a comprehensive understanding of the coordination structure of dominant copper species in both the extracted organic phase and ammoniacal solutions by X-ray absorption spectroscopy and DFT calculation. Along this line the structure and energy of a series of conformers of $[Cu(NH_3)_x(H_2O)_y]^{2+}$ (x+y = 4 or 6) in the gas phase were calculated at the B3LYP level to analyze their stability and the dominant structure of copper(II) species in ammoniacal solution. The configuration of the extracted copper complex in organic phases was found to be square planar and independent of the aqueous pH. When two and more ammonia molecules coordinate

with hydrated copper(II) in ammoniacal solutions, the coordination number of copper(II) species decreases and their geometries change from axially elongated octahedral to distorted square planar. The authors also proposed a probable microscopic mechanism of copper extraction in ammoniacal solutions shown in Fig. 4.

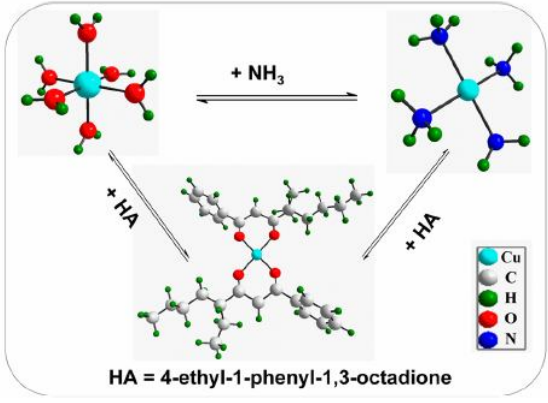

Fig. 4 Extraction mechanism of copper(II) in ammoniacal solution (reproduced with permission from ref. 92).

Copper corrole complexes (Fig. 5) were generally considered as typical low-spin diamagnetic copper(III) complexes.

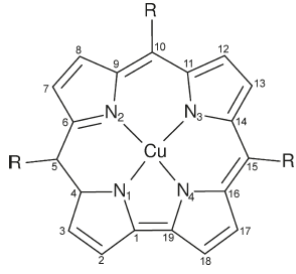

Fig. 5 Calculated structures: Cu(C) (R = H) and Cu(TPC) (R = C_6H_5) (reproduced with permission from ref. 96).

The first computational study,[93] carried out on unsubstituted copper corrole by means of DFT employing the PW91 DF, also confirmed the Cu(III) closed-shell d^8 character of the ground state, and identified the low-lying triplet state as originating from the excitation of an electron from the b_1 type corrole π orbital into the empty Cu 3d orbital. Later DFT calculations employing the B3LYP DF, pointing to an open-shell singlet ground state built from antiferromagnetic coupling between Cu(II) d^9 and a singly occupied corrole π orbital.[94] The antiferromagnetic coupling interaction was found to be the driving force for a saddling distortion of the corrolate ligand, allowing for attractive σ-π interactions between the two orbitals involved in the coupling. X-ray crystallographic analysis of two sterically unhindered copper mesotriarylcorroles, combined with DFT calculations using the

OLYP DF, confirmed that saddling is indeed an inherent feature of copper corroles.[95] The saddled structures calculated with the OLYP functional were found to have a closed-shell singlet ground state, rather than the (unphysical) spatial separation of positive and negative spin densities that is observed with B3LYP.[94]

More recently a comparative study of the electronic and geometric structure of copper corrole complexes, containing either unsubstituted corrole, Cu(C), or meso-triphenyl corrole Cu(TPC) by means of DFT and multi-configurational *ab initio* methods was reported by Pierloot et al.[96] The results obtained from DFT with four different DFs (BP86 and OLYP pure GGA, B3LYP and PBE0 H-GGA) were compared with those obtained from either the complete or restricted active space self-consistent field method (CASSCF or RASSCF), with dynamic correlation accounted for with second-order perturbation theory (CASPT2 or RASPT2). It was shown that the concrete description of the ground state electronic structure of these complexes heavily depends on the computational approach. DFT geometry optimizations were performed for the lowest singlet and triplet states of copper corrole complexes and the effect of saddling on the electronic structure was investigated by comparing the results obtained for planar (C_{2v}) and saddled (C_2) structures. In particular, pure GGA DFs (BP86, OLYP) predict a closed-shell ground state with strongly covalent copper-corrolate bonds, of pure σ type in the planar structure, but with strongly mixed σ-π character in the saddled structures. On the other hand, H-GGA DFs (B3LYP, PBE0) predict an open-shell singlet ground state with pronounced diradical character, built from magnetic exchange coupling between two unpaired spins in either Cu $3d_{x^2-y^2}$ and the b_1 type corrolate Highest Occupied Molecular Orbital (HOMO). The CASPT2 results essentially confirm the suggestion from the hybrid DFs that copper corroles are noninnocent, although the contribution of diradical character to the copper-corrole bond is found to be limited to 50% or less.

A DFT approach based on the UB3LYP DF and basis sets of different size and quality was used in order to elaborate a computational protocol providing a reliable quantitative estimate of the spin–spin interaction in two isomeric complexes of Cu(II) with acetylacetonate and isomeric aminoxyl radicals (3- and 4-*N*-oxyl-tertbutylaminopyridine), whose geometry and magnetic properties were known from experimental data.[97] The computational protocol allowed the elucidation of the role of various structural factors on the type and magnitude of the spin coupling, such as symmetry, spatial orientation of the radicals and type of the magnetic orbital of the metal ion.

DFT calculations on a series of binuclear cyclopentadienylcopper cyanides formulated as $Cp_2Cu_2(CN)_n$ ($Cp = \eta^5$-C_5H_5; n = 1, 2, 3) predicted that the lowest energy structures have terminal Cp rings and bridging cyanide ligands up to a maximum of two bridges, while higher-energy $Cp_2Cu_2(CN)_n$ (n = 1, 2, 3) structures have bridging Cp rings.[98] The $Cp_2Cu_2(CN)_2$ and $Cp_2Cu_2(CN)$ species, with the copper atoms in the average oxidation states +1.5 and +2, respectively, are predicted to have marginal viability. On the other hand, the $Cp_2Cu_2(CN)_3$ species, with the copper atoms in an average oxidation state of +2.5, are thermodynamically disfavored with respect to cyanogen loss. The prospects for the copper(II) derivative $Cp_2Cu_2(CN)_2$ contrast with that of the "simple" $Cu(CN)_2$, which is shown both experimentally and theoretically to be unstable with respect to cyanogen loss to afford CuCN.

2.3. DFT insights on the catalytic activity of copper coordination compounds

2.3.1. Copper(I)-catalyzed azide-alkyne cycloaddition. The copper-catalyzed azide–alkyne cycloaddition (CuAAC) reactions are the most broadly applicable and easy-to-handle reactions in organic chemistry. The CuAAC process has emerged as the premier example of a new branch in organic chemistry called "click chemistry", a term coined in 2001 by Sharpless to describe a set of 'near-perfect' bond-forming reactions useful for rapid assembly of molecules with desired function.[99] The history of the development of the CuAAC reaction, its key mechanistic aspects, and highlights the features that make it useful to practitioners in different fields of chemical science were presented in a tutorial review article by Hein and Fokin.[19] Recently Berg and Straub[100] summarized the development of the mechanistic understanding of the copper-catalyzed azide–alkyne cycloaddition from early proposals to a more sophisticated updated view based on results from kinetic and computational studies in the last decade. Therefore, it is intended herein to highlight the most recent mechanistic studies of the CuAAC's catalytic cycle carried out by DFT methods.

Computational studies on the Huisgen's 1,3-dipolar cycloadditions,[101] revealed a stepwise mechanism (Scheme 1) involving metallacycle intermediates, which appear to be common for a variety of dipoles.[102] The catalytic cycle begins with the formation of copper acetylide **2** followed by replacement of one of the ligands by the azide which binds to the copper atom via the nitrogen proximal to carbon, forming intermediate **3**. After that, the distal nitrogen of the azide in **3** attacks the C-2 carbon of the acetylide, forming the unusual six-membered copper(III) metallacycle **4**. Intermediate **4** is transformed to the triazolyl-copper derivative **5**, through a barrieles transition stat (activation barrier of 3.2 kcal/mol) and after protonolysis releases the triazole product, thereby completing the catalytic cycle.

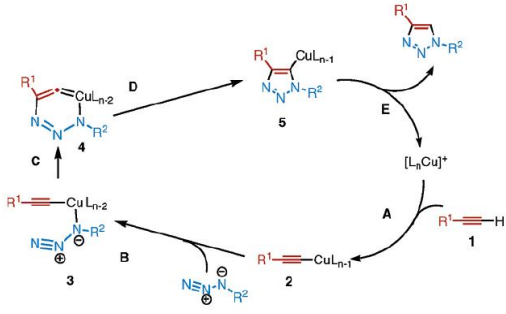

Scheme 1 Proposed reaction mechanism of the Huisgen's 1,3-dipolar cycloadditions (reproduced with permission from ref. 102).

The proposed mechanism accounts for the key experimental observations, i.e. the dramatic rate increase observed in the copper-catalyzed synthesis of 1,2,3-triazoles which is in excellent agreement with the computed activation barriers and the exclusive *regio*-selectivity of the copper(I)-catalyzed processes.

DFT calculations at the B3LYP/LACV3P++(d,p)//B3LYP/LACVP(d,p) level of theory revealed that dinuclear and tetranuclear copper acetylide complexes display both superior stability and higher reactivity in the CuAAC reaction than do mononuclear complexes.[103] Their existence rationalizes the observed second order

rate laws with respect to copper concentration since copper(I) alkenylidene complexes can be avoided as highly strained six-membered cyclic intermediates.

Cantillo et al.[104] assessed the whole range of the archetypal Cu(I)-catalyzed alkyne-azide click cycloaddition (CuAAC) mechanisms by DFT calculations, modeling copper nuclei with the LANL2DZ basis set and aqueous environments with CPCM solvation model. All of the proposed mechanisms, ranging from the intermediacy of copper acetylides to π-complexes and multinuclear clusters have been compared. An in-depth analysis of all the mechanistic proposals through DFT calculations showed that Cu-acetylides, in particular the two-metal center species, are the most plausible intermediates in accelerating the formation of triazoles. The computed energy barriers for the catalytic pathways mediated by these species (16.0 and 20.4 kcal mol^{-1} for the regioisomeric 1,4- and 1,5-approaches, respectively) explain the experimentally observed *regio*-selectivity as well as the significant rate acceleration.

Most recent DFT calculations showed that the nature of the mechanism for the CuAAC reaction depends on the ligands attached to Cu(I).[105] The *regio*-selectivity of mononuclear CuAAC was rationalized by means of analysis of the evolution of "atomic graphs" (Bader's definition) throughout the corresponding reaction coordinates. The topological evolution of the charge density, $\rho(\mathbf{r})$, the Laplacian of $\rho(\mathbf{r})$, $\nabla^2\rho(\mathbf{r})$, and its gradient field along the reaction coordinate shed light on the *regio*-selectivity of the process. An explanation of the dependence of the mechanism (concerted or stepwise) upon changing the ligand attached to Cu(I) was also outlined. For the acetonitrile ligand the LC-wPBE(PCM)/6-311++G(d,p) and M06-2X(PCM)/6-311++G(d,p) computational protocols predict a straight asynchronous concerted process connecting the acetylide complex to the five-membered ring product, without the participation of the six-membered metallocycle. The B3LYP(PCM)/6-311++G(d,p) computational protocol predicts a stepwise process for L = CH_3CN in both situations. This process becomes even more direct on the potential energy hypersurface calculated at the M06-2X(PCM)/6-311++G(d,p) level, where that region with null curvature does not appear to occur, but rather a tiny shoulder that links the transition state directly with the product. On the contrary, when the ligand was water (H_2O as solvent) or CH_3OH (CH_3OH as solvent) the LC-wPBE(PCM)/6-311++G(d,p) and wB97XD(PCM)/6-311++G(d,p) levels of theory, render a stepwise process.

2.3.2. Copper(I)-catalyzed cyclopropanation reactions. Cyclopropane rings perform a key structural role in a wide array of bioactive natural and synthetic products.[106,107] In recent years, efforts have been invested in the development of asymmetric cyclopropanation reactions via copper-catalyzed decomposition of diazo compounds followed by carbene insertion to olefins. The design and synthesis of various copper complexes bearing ligands with renowned chirality lead to successful diastereo- and enantio-control. The mechanism of the copper catalyzed cyclopropanation reactions of diazo compounds has remained controversial even for the nonchiral systems. However, two points of the mechanistic details are widely accepted:

(i) the actual catalyst is a Cu(I) species even if Cu(II) is used and
(ii) a short-lived electrophilic copper(I)-carbene is the reactive intermediate.

In other words, copper reacts with the diazo compound to generate a transient electrophilic copper-carbene complex through a σ-donation and π-back bonding.[108]

The non-bonding pair of electrons located in the sp^2 hybrid orbital of carbene carbon atom is donated to copper forming a σ-dative bond, while concomitantly copper donates an electron to the empty p orbital of the carbene forming a π bond. In the absence of an olefin, the carbene dimerizes, affording the *cis*- and *trans*- coupled products. In the presence of an olefin, the coordinated carbene is released from the Cu(I) complex and selectively adds to the double bond, forming the three-membered cyclic compound. It is clear that a deeper understanding of this mechanism would undoubtedly lead to the design of even better catalysts.

DFT calculations provided details of the catalytic cycle of copper catalyzed cyclopropanation reactions. The mechanism of the copper(I)-catalyzed cyclopropanation reaction has been extensively investigated for a medium-size reaction model by means of B3LYP/6-31G(d) calculations.[109] A thorough examination of the free energy surface of a model reaction studied (Fig. 6) provided insights on the key steps of the catalytic cycle of copper-catalyzed cyclopropanation reactions. Accordingly, the starting species is a 1:1 catalyst-ethylene complex. In this complex ethylene can be replaced by the diazo ester through an associative displacement followed by extrusion of dinitrogen to yield a metal-carbene complex in a process that corresponds to the rate-limiting step. Calculations indicate that a direct carbene insertion is favored over a stepwise process in the step that controls the stereoselectivity. The formation of the catalyst-product complex is greatly favored for the cyclopropanation step. The regeneration of the catalyst-ethylene complex takes place through an associative displacement. DFT calculations on chiral bis(oxazoline)-Cu(I) system models revealed that steric interactions between the ester group and one of the substituents of the bis-(oxazoline) ligand determines the enantioselectivity, while the *cis/trans* selectivity in the final cyclopropanes is governed by the steric interaction between the carbene ester group and the substituents on the olefinic double bond.

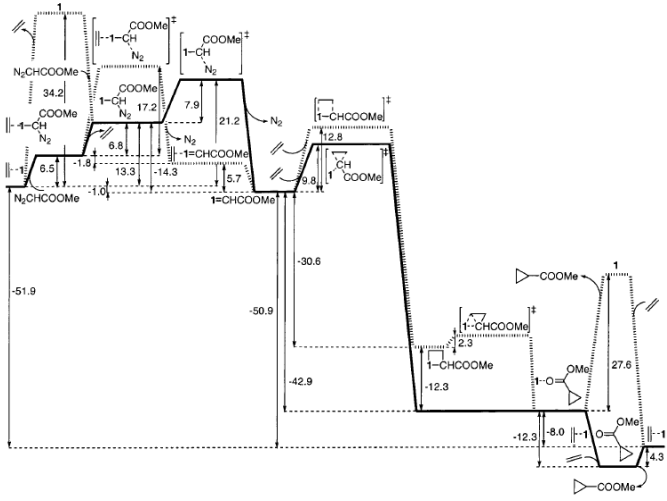

Fig. 6 Energy diagram for a catalytic cycle. The favored mechanism represented by solid lines and the alternative pathways by hashed lines (reproduced with permission from ref. 109).

According to Straub et al.[110] the copper(I)-olefin complex in copper-catalyzed cyclopropanation is the resting state of the catalytic cycle, which is in agreement with kinetic investigations. The existence of pre-equilibrium can be attributed to the copper(I)-diazoalkane complex, copper(I)-olefin complex, free diazoalkane and free alkene. All theoretical studies agree on the central role to the copper(I)-carbene as the reactive species, which is formed after N_2 extrusion. The computed intermediates and transition states of the catalytic cycle are closed-shell diamagnetic copper(I) or copper(III) complexes, in accordance with experimental data of observed or isolated intermediates.

The enantioselectivity in the reaction of [Cu(adam-box)($CHCO_2Me$)] {adam-box = 2,2′-isopropylidenebis[(*4R*)-(1-adamantyl)-2-oxazoline]} with $Ph_2C{=}CH_2$ was analyzed computationally by ONIOM(B3LYP:UFF) calculations.[111] The authors defined possible reaction paths in the Gibbs free-energy surface that allowed the Gibbs free-energy barriers leading to the *R* and *S* products to be estimated. The computed enantiomeric ratio is heavily in favor of the *S* product, which is in good agreement with experiment. The overall enantioselectivity depends on the balance of several different contributions: (i) the relative orientation of the carbene and bis(oxazoline) planes, (ii) the steric repulsion between the ester and adamantyl substituents, and (iii) the steric repulsion between the olefin phenyl substituents and both the adamantyl groups and the bis(oxazoline) system.

Recently, an extensive computational study employing various DFT schemes has been carried out on different catalytic systems for cyclopropanation reactions based on copper.[112] Among the density functionals used, PBE, M05 and M06 are the best performers predicting accurate absolute kinetic properties (energy barriers) of such systems. Most of the computational protocols used tend to overestimate activation barriers, allowing the location of the transition state on the PES of the most reactive systems, which are probably artifacts of the method. However, after a thorough analysis of the calculated PES, and the origin of the energy differences obtained for the different alkene approaches in chiral systems, it was found that energy differences are almost constant over a wide range of geometries covering the reaction channel zone in which the true TS on the Gibbs free energy surface lies.

A new methodology to quantitatively assess the enantioselectivity of asymmetric catalysis based on quantitative quadrant-diagram representations of the catalysts and quantitative structure–selectivity relationship (QSSR) modelling was provided by Aguado-Ullate and co-workers.[113] The methodology was applied to predict the enantioselectivity in the cyclopropanation of styrene catalysed by copper complexes. The dataset comprised 30 chiral ligands belonging to four different oxazoline-based ligand families: bis- (Box), azabis- (AzaBox), quinolinyl- (Quinox) and pyridyl-oxazoline (Pyox). They found that the relationship between the steric hindrance and the enantioselectivity is non-linear, and that bulky substituents in diagonal quadrants operate synergistically.

2.3.3. Copper(I)-catalyzed cross-coupling reactions. The discovery of transition-metal mediated reactions for the synthesis of carbon-carbon and carbon-heteroatom bonds was an important discovery for synthetic chemists. Since the original work of Ullmann and Goldberg,[114-116] it has been known that various copper sources are effective in the C–C and C–X coupling reactions, ranging from Cu(I) to Cu(II) salts, and even including metallic copper. General aspects on the mechanism of the modified Ullmann reaction have recently been reported.[117] Four different

classes of mechanisms proposed for the Ullmann condensation reaction involve:

1. Oxidative addition of ArX on copper(I) resulting in an intermediate Cu(III) species.
2. Aryl radical intermediates, either *via* single electron transfer (SET) or *via* halide atom transfer (AT).
3. σ-bond metathesis through a four-centre intermediate.
4. π-complexation of copper(I) on ArX.

In the first two alternatives the copper species changes its oxidation state during the catalytic cycle, whereas in the last two the copper species maintains the same oxidation state through the whole cycle.

Guo and co-workers[118] explored the mechanism of the copper(I)-catalyzed reaction between phenyl bromide and acetamide by DFT calculations augmented with the CPCM solvation model. Comparison of multiple reaction pathways revealed that diamine-ligated copper(I) amidate was the most reactive intermediate in the reaction mixture for the oxidative addition to aryl halide. In addition, the DFT calculations pointed to the oxidative addition of ArX on $L_2Cu(I)$-amidate as the rate-limiting step, to generate a penta-coordinate $(Ar)(X)(amidate)L_2Cu(III)$ species.

The complete catalytic cycle of the coupling reaction of propylene oxide with carbon dioxide employing copper(I) cyanomethyl, $NCCH_2Cu$, as an active catalyst has been investigated at the B3LYP level of theory.[119] The overall catalytic reaction corresponds to a stepwise reaction which includes two processes. In the first process, CO_2 insertion into the Cu(I)-C bond of (cyanomethyl)copper(I) complex affords activated CO_2 carriers. In the second process, propylene oxide is coordinated to the electrophilic copper center of carriers via the O-donor atom. The theoretical results explain satisfactorily why $NCCH_2Cu$ plays an important role in the formation of propylene carbonate at high temperature.

DFT calculations were employed to discriminate between four different mechanisms (Scheme 2) of the Cu(I)-catalyzed reactions between iodobenzene and both methanol and methylamine.[120]

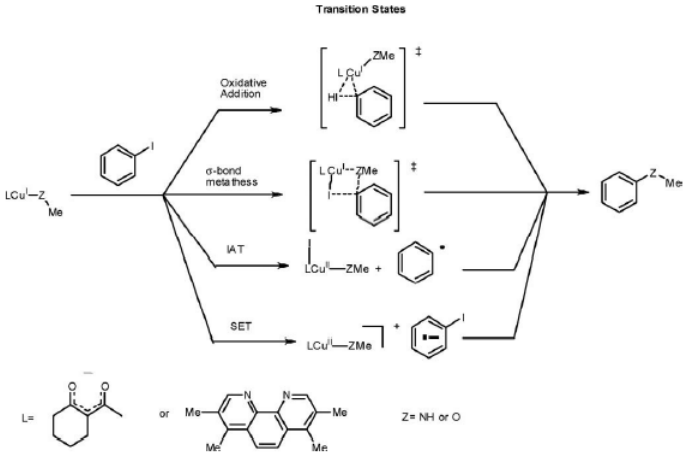

Scheme 2 Four mechanisms explored using DFT calculations (reproduced with permission from ref. 120).

The reaction with the aryl iodide calculated for both ligand types and nucleophiles for all four mechanisms was found to be the rate-determining step. The phenanthroline ligand promotes O-arylation reactions via IAT mechanisms in preference to N-arylation reactions, which occur via SET mechanisms in full agreement with experimental results. SET mechanisms are favored in reactions promoted by the β-diketone ligand; N-arylation is predicted to be favored in these cases, in agreement with experimental results.

Ranjit and co-workers[121] presented a general and highly efficient method for C−S cross-coupling through direct functionalization of a heterocyclic C−H bond with aryl or alkyl thiols in the presence of copper(I) catalyst. DFT calculations provided mechanistic details on the Cu(I)-mediated direct thiolation reactions (Scheme 3). The first reactive intermediate in the thiolation reactions is a Cu-thiol complex instead of the generally accepted Cu-thiazole complex. The authors postulated that molecular oxygen participates in the reaction by abstracting the hydrogen from the C-2 carbon of the thiazole to afford the Cu-hydroperoxo species. The computational studies revealed that a stepwise reaction mechanism based on a hydrogen atom abstraction pathway, is more energetically feasible than many other possible pathways including *β*-hydride elimination, single electron transfer, hydrogen atom transfer, oxidative addition/reductive elimination, and *σ*-bond metathesis.

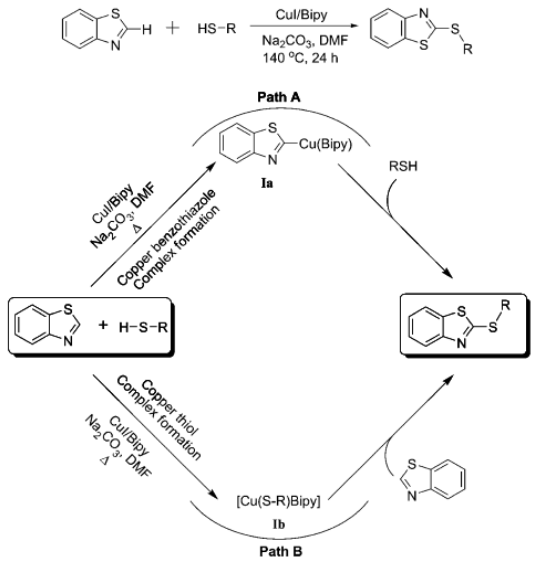

Scheme 3 Proposed reaction pathways (reproduced with permission from ref. 121).

The reaction mechanism of the Sonogashira cross-coupling, a multistep process, consisting of oxidative addition, *cis-trans* isomerization, transmetalation, and reductive elimination, was computationally modelled at the B3LYP/cc-pVDZ level of theory for reaction between bromobenzene and phenylacetylene, both in the gas phase and in dichloromethane solution using PCM method.[122] The rate-limiting step was found to be the oxidative addition process, correlating well with recent experimental data. The second crucial step of the catalytic cycle is the transmetalation step, which might be initiated by dissociation of the neutral ligand.

In a recent tutorial review Jiao and co-workers[123] highlighted numerous important advances that have been achieved in the development of copper-catalyzed dehydrogenative functionalization via a single electron transfer (SET) process including C–C, C–N, C–O, C–halogen, C–P, and N–N bond formation. The details of functions of the copper catalyst in some transformations have not been clarified yet, especially in the oxygen incorporation process. Along this line, theoretical and experimental investigations of the mechanistic details of these reactions are expected to improve the design and discovery of new highly active and selective catalysts for the application of copper-catalyzed dehydrogenative functionalization via a single electron transfer (SET) process.

The reaction mechanism of the copper-catalyzed cross-dehydrogenative coupling (CDC) reaction involving sp^3-C-H bond activation was studied by DFT calculations at the M06/6-311+g(d,p) level of theory.[124] Three pathways, namely the radical pathway, the Cu(III) pathway, and the SET pathway were calculated to have comparable activation free energies. Computational studies support the prevalent SET mechanism, but also uncovered an alternative mechanism (in blue) in which O_2 is directly involved in the C-H abstraction step (Scheme 4). Both of these two mechanisms are in good agreement with the experimental deuterium kinetic isotope effect (KIE).

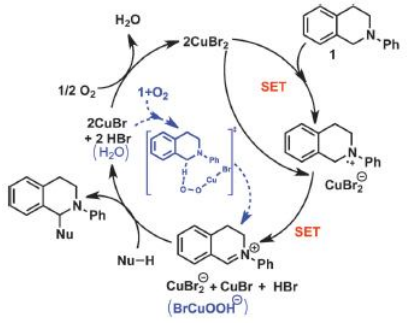

Scheme 4 Catalytic cycle for the SET mechanism (black) and an alternative mechanism in which O_2 is directly involved in the C-H abstraction step (blue) (reproduced with permission from ref. 124).

The effect of low copper concentrations in Sonogashira–Hagihara-type couplings of aryl halides and terminal alkynes along with the mechanistic aspects of the reaction were investigated by Bolm and co-workers[125] employing kinetic measurements and DFT calculations. The latter suggests that the reaction proceeds by a concerted breaking of the phenyl iodide bond and formation of the new C-C bond, and that this is the rate-liniting step. Calculations on various electronically modified systems reproduced the experimentally observed trends.

The mechanisms of the Cu(I)-mediated domino reaction of asymmetrical alkynes with LCuH (L = N-heterocyclic carbene) by the reducing reagent of hydrosilane, $HSi(OEt)_3$, was theoretically studied with the aid of DFT calculations using the B3LYP functional.[126] The calculations showed that coupling of alkynes with LCuH was the selectivity-determining step, though not the rate-determining step. The coupling reactions of LCuH with the four model alkynes (PhC≡CMe, PhC≡C^{t}Bu, AnC≡C^{t}Bu (An = anisole), and MbC≡C^{t}Bu (Mb = methyl-benzoate) gave the same regioselectivity, although the four alkynes are very different in terms of their

electronic properties and steric properties. The observed *regio*-selectivity is dominated by both electronic and steric factors.

Jiménez-Osés et al.[127] elucidated the stereochemical course of the copper-catalyzed C−H insertion of diazo compounds into cyclic ethers through a synergistic experimental and theoretical study. DFT calculations at the B3LYP/6-31G(d) and B3LYP/TZVP levels of theory augmented with the SMD solvation model were used to predict the stereochemical outcome of the bis(oxazoline)copper-catalyzed C−H insertion reaction between methyl diazophenylacetate and tetrahydrofuran and also to predict the absolute configuration of the major stereoisomers derived from the same reaction with different cyclic ethers. The observed stereoselection arises from a balance of stereoelectronic factors in which major roles play (i) the repulsive interactions between the ester group and the alkyl/aryl groups of the oxazoline rings, and (ii) the attractive van der Waals interactions between the substrates and the ligand. The absolute configuration of all the stereogenic centers present on the molecule is affected through a proposed ring-opening/cyclization process, leading to a complete loss of asymmetry.

2.3.4. Copper(I)-catalyzed hydrosilylation reactions. Enantioselective copper(I)-catalyzed reductions rank among the valuable and broadly applicable C-H bond-forming reactions.[128] In a landmark publication dating back almost a quarter of a century, Brunner and Miehling reported on the first copper(I)-catalyzed reduction of acetophenone using diphenylsilane as the reducing reagent.[129] The copper-catalyzed asymmetric hydrosilylation of ketones is an efficient method for the synthesis of chiral enantiopure secondary alcohols. The catalytic cycle suggested for the hydrosilylation of ketones by Cu(I) hydrides has been investigated by DFT methods, using a model system made up of a $CuH(PH_3)_2$ catalyst, acetone and SiH_4.[130] The catalytic activity of the more rigid $CuH[C_4H_4(PH_2)_2]$ catalyst, as well as tetra-coordinated, $CuH(PH_3)_3$ and $CuH(PH_3)[C_4H_4(PH_2)_2]$ compounds were also evaluated. The CuF_2 precatalyst used is activated by refluxing a CuF_2/PPh_3 mixture in methanol to afford the $FCu(PPh_3)_3$ complex, which through ligand exchange reactions with diphosphane, $Ph_2PCH_2CH_2PPh_2$, ligands yields the $CuF(PPh_3)_n[(C_4H_4(PPh_2)_2]$ complex. The latter reacts with the hydrosilane R_3SiH to yield the catalytically active $CuH(PPh_3)_n[(C_4H_4(PPh_2)_2]$ species, which enters in the catalytic cycle (Scheme 5). The transition states are characterized by an increase in bond length of those bonds that are breaking, and a decrease in bond length of the newly formed bonds. Calculations showed that both steps of the actual catalytic cycle exhibiting a free energy barrier of about 10 kcal/mol confirm the plausibility of the suggested cycle.

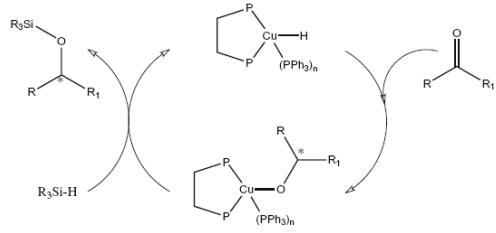

Scheme 5 Catalytic cycle for the hydrosilylation of ketones catalyzed by Cu(I) hydrides (reproduced with permission from ref. 130).

A detailed DFT computational study, employing the B3LYP functional, of the copper(I)-catalyzed asymmetric hydrosilylation of ketones was presented by Dedieu and co-workers.[131] The proposed overall catalytic cycle is shown in Scheme 6.

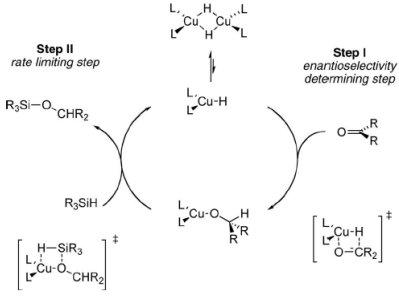

Scheme 6 Catalytic cycle displaying the two steps in the coppercatalyzed hydrosilylation process (reproduced with permission from ref. 131).

The DFT calculations suggest that the insertion of the ketone into the Cu–H bond is the enantioselectivity determining step (Step I). Step II, which corresponds to the reaction of the copper alkoxide with the silane to form the silyl product and regenerate copper hydride, is found to be the rate-determining step. The insertion of the ketone into the Cu–H bond was found to have a lower activation barrier than the reaction of the copper alkoxy intermediate with the silane, which regenerates Cu–H along with the silyl ether product. Noteworthy the reaction occurs only in the presence of a silane, which is the driving force of the reaction leading to the formation of a stable silyl ether product.

In two recent publications Vergote and co-workers[132,133] investigated the plausibility of the catalytic cycle suggested for the hydrosilylation of ketones by (NHC) copper(I) hydrides by DFT methods. Computations showed the activation of the CuF_2 pre-catalyst, as well as both steps of the catalytic cycle to involve a four-center σ metathesis transition state as suggested in the literature. Both steps of the actual catalytic cycle exhibit a free energy barrier of about 14.5 kcal/mol for the largest IPr (IPr = 1,3-bis(2,6-diisopropylphenyl)imidazol-2-ylidene) N-heterocyclic diaminocarbene (NHC) ligands. The authors also demonstrated that the (NHC)CuF species are active catalysts that do not require an activating agent. The self activating mechanism of a (NHC)CuF pre-catalyst has been elucidated by a combined theoretical and experimental study. Several hypotheses on the activation mechanism have been investigated, and experimental and theoretical results, point towards the formation of a tight ion pair between a difluorosilicate and a cationic copper(I) complex.

The copper-catalyzed reaction among PhC≡CPh, CO_2 and $HSi(OEt)_3$ has been theoretically investigated by means of DFT calculations, with the aim to make clear why the reaction prefers a hydrocarboxylation process rather than a hydrosilylation one.[134] For the hydrocarboxylation process, CO_2 insertion into Cu-C bond of the copper alkenyl complex and the subsequent σ bond metathesis between Cu-O and H-Si were proved kinetically feasible under the reaction conditions. The metathesis process was found to be the rate-determining step with activation barrier of 30.1 kcal/mol. For the hydrosilylation process, the σ bond metathesis between Cu-C and H-Si was found to be kinetically unavailable with activation barrier of 47.4 kcal/mol

in the presence of CO_2. The formation of the more stable CO_2 insertion product, H(Ph)C=C(Ph)CO_2CuL, plays an important role in blocking the reaction to undergo hydrosilylation.

2.3.5. Copper(I)-catalyzed oxygenation reactions. Oxidative and oxygenation reactions with copper catalysts and reagents that employ O_2 as the terminal oxidant confer a remarkably broad range of activities toward sustainable and environmentally benign synthetic methods. A recent elegant review comprehensively covers copper-catalyzed oxidation chemistry using oxygen as the oxidant up through 2011, providing also the current mechanistic hypothesis for each reaction.[135] However, understanding of the basic chemical steps involving copper in these mechanisms employing DFT methods are limited. Much is still unknown about the reaction of copper complexes with molecular oxygen under different sets of conditions. As the understanding of the fundamental mechanisms of copper-catalyzed oxidative and oxygenation reactions improves, the prospects for achieving new or improved oxidative processes are very promising.

Copper is found in the active site of many metalloenzymes that catalyze aerobic oxidation reactions. These enzymes include "oxygenases", which mediate oxygen-atom transfer to organic substrates, and "oxidases", which couple the reduction of O_2 to the oxidation of diverse substrates. A number of important synthetic Cu-catalyzed aerobic oxidation reactions exist, including industrial applications.[136]

Oxidative functionalization of C-H bonds is one of the most challenging classes of oxidation reactions. Stahl and co-workers[137] highlighted the broad array of Cu-catalyzed aerobic C-H oxidation reactions and clarified key challenges that lie ahead. Kinetic and in situ spectroscopic studies of the Cu^{II}-catalyzed C−H methoxylation and amidation of a macrocylic arene substrate with O_2 as the stoichiometric oxidant demonstrated the involvement of three different oxidation states of Cu in the catalytic mechanism (Scheme 7), including an aryl-Cu^{III} intermediate.[138] The mechanistic details of a mild aromatic C−H activation effected by a copper(II) center ligated in a triazamacrocylic ligand, affording equimolar amounts of a Cu^{III}-aryl species and Cu^{I} species as reaction products.[139]

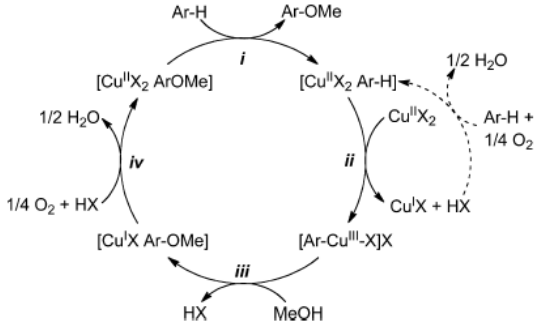

Scheme 7 Proposed catalytic cycle for Cu-catalyzed aerobic oxidative methoxylation of a macrocyclic arene (reproduced with permission from ref. 138).

At low temperatures the Cu^{II} complex forms a three-center, three-electron C−H···Cu^{II} interaction, identified by pulse electron paramagnetic resonance spectroscopy and supported by DFT calculations. C−H bond cleavage is coupled

with copper oxidation, as a Cu^{III}-aryl product is formed. This reaction proceeds to completion through either a copper disproportionation reaction or, alternatively, even faster with 1 equiv of 2,2,6,6-tetramethylpiperidine-1-oxyl (TEMPO), quantitatively yielding the Cu^{III}-aryl product. Kinetic studies of both reactions strongly implicate a rate-limiting proton-coupled electron transfer (PCET) as the key C−H activation step, a mechanism that does not conform to any previously proposed C−H activation mechanisms.

Poater and co-workers[140] reported a complete and detailed mechanism for the σ* intramolecular aromatic hydroxylation through O_2 activation by a hexaazamacrocyclic dicoppper(I) complex, $[Cu_2(H3m)]^{2+}$ by means of DFT (B3LYP) calculations. The H3m hexaazamacrocyclic ligand has the formula:

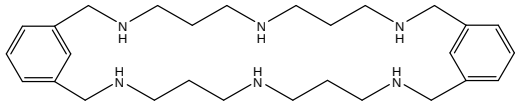

The computational results indicated that a Cu(I)-Cu(II) superoxo species is formed first, then the interaction of the O_2 moiety with the second Cu(I) center leads to a μ-η^2:η^2-peroxo-Cu_2(II) intermediate. The B3LYP calculations indicated also that it is the, μ-η^2:η^2-peroxo species that evolves via an electrophilic σ* attack involving a concerted peroxide O-O bond cleavage and C-O bond formation to a Wheland-type intermediate. The reaction proceeds with a proton release assisted by the presence of a second aromatic ring yielding a μ-hydroxo- μ-oxo intermediate species, which, in the final stage of the reaction, rearranges to the product. The lack of high energy barriers and deep energy wells explain the difficulty to trap intermediates experimentally.

The reactivity of a mononuclear Cu(II)-hydroperoxo species bearing a pentadentate N5 ligand, with general formula $[Cu^{II}(N4Py)(OOH)]^+$ (N4Py = *N*,*N*-bis(2-pyridylmethyl)bis(2-pyridyl)methylamine) has been investigated both experimentally and theoretically.[141] DFT calculations at the B3LYP/LACVP(Cu) $\cup$ 6-31G*(E) augmented with the polarized continuum model (PCM) provided mechanistic details on the epoxidation of ethylene by $[Cu(N4Py)(OOH)]^+$ and a $[Cu^{III}(N4Py)(O)]^+$ intermediate. The estimated activation barrier for the olefin epoxidation by the Cu(II)-hydroperoxo species is high, indicating that this intermediate is not capable of oxygenating olefins. In other words the mononuclear Cu(II)-hydroperoxo species bearing a pentadentate N5 ligand is a sluggish oxidant in oxygenation reactions. In contrast, the Cu-oxo complex easily mediates the olefin epoxidation with a low energy barrier, but the homolytic cleavage of the O-O bond of the Cu-hydroperoxo complex to form the Cu-oxo species is very endothermic.

The mechanism for the oxygenation of Cu(I) complexes with α-ketocarboxylate ligands was explored by DFT and multireference second order perturbation theory (CASSCF/CASPT2) calculations.[142] The reaction proceeds by initial attack of a coordinated O_2 molecule on a ketocarboxylate ligand with concomitant decarboxylation followed by formation of two reactive intermediates, a Cu-peracid structure, (N^N)CuOOC(O)R, and a $[RC(O)OCuO]^+$ species, both being capable of oxidizing a phenyl ring that is a component of the supporting ligand. Hydroxylation by the $[RC(O)OCuO]^+$ species is predicted to proceed with a smaller activation free energy.

The full reaction mechanism of the hydroxylation of phenols mediated by the μ-

η^2:η^2-peroxodicopper(II)(DBED)$_2$ (DBED is N,N′-di-tert-butylethylenediamine) $[Cu_2O_2(DMED)_2]^{2+}$ complex has been investigated by DFT methods using the hybrid B3LYP functional and replacing the DBED by N,N′-dimethylethylenediamine (DMED) ligands to reduce the computational costs.[143] The proposed reaction mechanism follows an electrophilic aromatic substitution pattern that involves an intermediate with the O–O bond cleaved and the phenolate coordinated to a copper center. The rate-determining step for the hydroxylation of this intermediate to the final products is the attack of one oxygen atom of the Cu_2O_2 unit on the aromatic ring leading to a new C–O bond.

The mechanism of the oxidation of inert alkane C−H bonds providing alcohols and/or ketones as the major products but inducing the dehydrogenation of these substrates catalyzed by [Tp^{x}Cu(NCMe)] (Tp^x = hydrotrispyrazolylborate ligand) complexes has been explored by experimental and DFT methods.[8] DFT results support a copper-oxo active species, which initiates the reaction by H abstraction. Spin crossover from the triplet to the singlet state, which is required to recover the catalyst, affords the major hydroxylation and minor dehydrogenation products. The calculations indicated that the superoxo and hydroperoxo species are less reactive than the oxo ones. A complete mechanistic proposal in agreement with all experimental and computational data was presented. According to the proposed mechanism the Tp^{x}Cu core reacts with hydrogen peroxide to give a copper-oxo intermediate with strong oxyl character. Interaction with cyclohexane induces a hydrogen abstraction process yielding the cyclohexyl radical and Tp^{x}Cu−OH. Next, two competitive pathways may occur: (i) the hydroxylation pathway which involves the collapse of the cyclohexyl radical with Tp^{x}Cu−OH leading to cyclohexanol formation, and (ii) the dehydrogenation pathway, which involves a second hydrogen abstraction from the α C−H of the cyclohexyl radical leading to cyclohexene formation. These pathways involve spin crossover through minimum energy crossing points (MECPs) of similar energy, which leads to product mixtures.

Recently, Pederes *et al.*[144] examined the mechanism of the copper(II)-promoted olefin amino-oxygenation reaction by means of a combined experimental and theoretical study. Kinetics experiments revealed a mechanistic pathway involving an equilibrium reaction between a copper(II) carboxylate complex and the γ-alkenyl sulfonamide substrate followed by intramolecular *cis*-addition of N-Cu across the olefin, the later being the rate-limiting step. Kinetic isotope effect (KIE) studies support that the *cis*-aminocupration is the rate-determining step. The EPR experiments and DFT calculations illustrated the possible contribution of nitrogen radical chemistry in the mechanism and conclusively eliminate the involvement of a nitrogen radical in the productive steps of the reactions mechanism. Two mechanistic scenarios were envisioned for this amino-oxygenation reaction, which differ in their possible starting [N-Cu] complexes, in particular, the number of coordinated acetate ligands. Path A starts from [(R^{1}R^{2}N)Cu(OAc)(HOAc)] (R^1 = tosyl (Ts), R^2 = 2-allylphenyl) and is the two-acetate, neutral path. Path B starts from [(R^{1}R^{2}N)CuOAc] + HOAc and is the one-acetate, neutral path. It was found that one-acetate-ligand mechanism (path B) has a lower aminocupration activation barrier than the two-acetate neutral mechanism (path A) by about 1.2 kcal/mol.

The origin of the enantioselectivity in the [Cu(*R*,*R*)-Ph-box](OTf)$_2$-catalyzed intramolecular amino-oxygenation of γ-unsaturated sulfonamides to afford chiral indolines and pyrrolidines, respectively, was investigated by means of DFT calculations.[145] The favored pro-(S) transition states (TSs) contain copper(II) centers

with distorted square-planar geometries, while the minor pro-(R) TSs contain copper(II) centers with geometries more consistent with distorted tetrahedral coordination. The major pro-(S) TSs adopt chairlike seven-membered cyclization conformations, while the minor pro-(R) TSs adopt boatlike seven-membered cyclization conformations. Calculations showed that the substrate's N-sulfonyl group plays a significant role in the reaction's enantioselectivity, which was further observed by changes in selectivity with changes in the N-sulfonyl group. The sterically demanding sulfonamide moiety makes alternative minor chair-like TSs more energetically demanding.

2.4. DFT insights on the bioactivity of copper coordination compounds

There are many theoretical and experimental studies exploring the bioactivity of copper coordination compounds and copper proteins. Siegbahn and Wirstam[146] investigated the redox process on tyrosinase. Latter on Prabhakar and Siegbahn[147] studied the molecular mechanism of the oxidation reaction on a center of copper amine oxidase by DFT calculations employing the B3LYP hybrid DF. A systematic investigation of the Cu(I)/Cu(II) cation interactions with biologically important types of ligands (water, ammonium, and hydrogen sulfide) with general formula $[Cu(H_2S)_m(H_2O)_n(NH_3)_k]^{2+}$ (where *n*, *m*, and *k* are equal to 0, 2, 4, and 6, along with the restriction $m + n + k = 4$ or 6) at the B3PW91/6-31G(d) level was performed by Burda and co-workers.[148] Energy decomposition analyses revealed that ammine complexes are the most stable, followed by those containing the aqua and hydrogen sulfide ligands, which are characterized by similar stabilization energies and the most preferred Cu(I) coordination number is two in ammine or aqua ligand fields, while for complexes with H_2S ligands the four-coordination is favored. In a subsequent paper Pavelka and Burda[149] reported the results of DFT calculations at the B3LYP/6-31+G(d) level on models of mononuclear centres of the active sites of blue copper proteins in both reduced and oxidized states. The authors examined two families of these redox sites, the Type A centres with general formula $Cu(Cys)_2(His)(Met)$ (Cys = Cysteine, His Histidine, Met = methionine) and the Type B with general formula $Cu(Cys)_2(His)$(Glh = glutamine). The family of Type A centres includes the peptides, amicyanin, auracyanin, plastocyanin, and rusticyanin, while family of Type B centres includes mavicyanin, stellacyanin, and umecyanin proteins. Both reduced and oxidized states were investigated in the gas phase as well as in the implicit solvent regime employing the COSMO solvation model simulating water ($\varepsilon = 78$) and protein-like environment ($\varepsilon = 4$). Detailed insight into the properties of these Cu(I)/Cu(II) complexes was provided by energy decomposition analyses performed at the more accurate B3LYP/6-31++G(2df, 2pd) level. Comparing relative difference between the constrained A and B protein's centres, the redox potential difference $\Delta E^0 = 0.20$ eV was obtained, which is in accord with experimentally known data (~ 0.14 eV). Natural population analyses (NPA) revealed that most of the spin density (80–90%) is located on the Cu–S(Cys) bond. The B centres exhibit a higher portion of spin density on Cu as well as a higher partial charge localized on the Cu atom compared to the A centres. Such behavior reflects the stronger ability of the glutamine ligand to donate electron density compared to the methionine ligand.

The superoxide dismutase (SOD) mimetic activities of novel mixed ligand complexes of copper with nicotinic and other selected carboxylic acids (phthalic,

salicylic and anthranilic acids) were observed to correlate well with theoretical parameters calculated at the B3LYP/LANL2DZ level of theory.[150] It was found that the SOD activity of the copper complex CuNA/Ph was positively correlated with the electron affinity (EA). Moreover, the highest occupied molecular orbital (HOMO) and lowest unoccupied molecular orbital (LUMO) eigenvalues correlate also well with the SOD activity. These findings demonstrated a great potential for the development of value-added metallovitamin-based therapeutics.

DFT calculations at the BP86/QZ4P(Cu) ∪ TZ2P(E) (E = main group element) level using the zeroth-order regular approximation (ZORA) have been performed on $[Cu(phen)_2]^{2+/+}$ and a series of six different $[Cu(Clip\text{-}Phen)]^{2+/+}$ complexes (Scheme 8), with or without a coordinating chloride ligand, to evaluate the influence of the length and functional substituents of the bridge linking the two phenanthroline units on the DNA cleavage activity.[151]

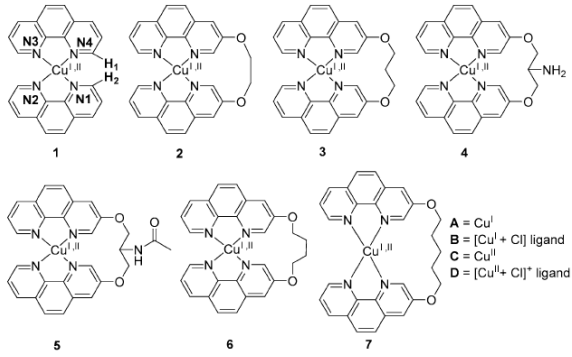

Scheme 8 The optimized structures of complexes **1** $Cu(phen)_2$, **2** Cu(3-ethyl-Clip-Phen), **3** Cu(3-propyl-Clip-Phen), **4** Cu(3-Clip-Phen), **5** Cu(3-acetyl-Clip-Phen), **6** Cu(3-butyl-Clip-Phen) and **7** Cu(3-pentyl-Clip-Phen) were calculated for the two oxidation states and with or without chloride as a fifth ligand, namely Cu^I (**A**), [Cu^I–Cl] (**B**), Cu^{II} (**C**) and [Cu^{II}–Cl]+ (**D**). The nitrogen atoms close to the bridges are numbered N1 and N4 (reproduced with permission from ref.151).

The calculations revealed that the bridge length of these complexes is critical for the consequent geometry, and both the strain and ligand binding energies. Upon reduction (needed for the DNA cleavage activity), the geometry of $Cu(phen)_2$ changes drastically. An unambiguous relation between the number of methylene groups constituting the bridge and the strain energy is observed: the highest energies are observed with the shortest bridges, and vice versa. For the redox properties of the complexes, no correlation is observed with their cleaving abilities. The different cleaving abilities observed can be explained as follows: (i) a shortening of the bridge gives rise to an increase of the planarity of the resulting Cu(I) complexes, which is reflected by a subsequent higher affinity for DNA, and (ii) the structural changes occurring upon oxidation or reduction are less dramatic for the complexes possessing a short bridge.

Ruiz-Azuara and co-workers[152] studied the interaction between mixed chelate complexes with traditional name Casiopeínas®, such as the Casiopeína III-ia formulated as [Cu (4,4′-dimethyl-2,2′-bipyridine)(acetylacetonate)(H_2O)]NO_3 with adenine cytosine, thymine and guanine in order to understand the nature of stacking

interactions in the system. X-ray and DFT calculations at the M05-2X/LANL2DZ level revealed that the stacking interactions are due to several π–π and C–H$\cdots\pi$ interactions between the Casiopevna's ligands and adenine molecules accompanied by a charge transfer of 0.06 $|e|$ from the adenines to the Casiopeína III-ia with a slight participation of the copper center. The affinity r of Casiopeína III-ia to DNA bases follows the order: G > C > A > T. The stacking mechanism between adenine molecules and Casiopeína III-ia can be understood as electron redistribution in the supramolecule, which stabilize the adenine adduct. In a next paper, Ruiz-Azuara's group [153] suggested that Casiopeínas® can intercalate between DNA base pairs through their aromatic moiety and that the π-stacking interaction is driven by an electron depletion of the planar bipyridine or phenanthroline ligand due to the transfer of charge to the metal center which, in turn, drives charge transfer from the flanking DNA bases to the intercalating ligand. Furthermore, the simple correlation between the complex stabilization energy of the adenine–Casiopeínas complex and the net electron population transferred from adenine to the aromatic ligand lends numerical support to the charge-transfer assisted π-stacking hypothesis and enhance the plausibility of the proposed mechanism of action initiated by stacking intercalation of Casiopeínas® between DNA base pairs. Two different anticancer mechanisms of Casiopeínas® were proposed. There might be antiradical molecules preventing the formation of cancer cells or these molecules could reduce the amount of GSH and as a result over-produce free radicals, increasing the oxidative stress which in turn kills the cancer cells.

The specific site of recognition between the Casiopeínas (*Cas*) formulated as $[Cu(2,2'\text{-bipyridine})(acetylacetonate)(H_2O)]^+$ and DNA was determined by molecular dynamics simulations and quantum chemical calculations.[154] The formation of the *Cas*–deoxyribose-phosphate adduct in the minor groove proves to be a good candidate toward the cleaving of DNA chains. *Cas* links to O1P and interacts with the deoxyribose by means of C–H$\cdots\pi$, O$\cdots$p(C) and O$\cdots$p(N) interactions between the sugar group and the aromatic ligand. The computational results indicate that the adduct *Cas*–deoxyribose-phosphate may be an initial step toward the hydrolysis of DNA chains and provide insights into the initial step of the action mechanism of copper complexes as apoptosis-inducing agents. The copper atom present in the *Cas* molecule may act as a catalysτ for the hydrolysis reaction, decreasing the atomic electron population of the phosphorous atom, which facilitates a direct attack by a nucleophile.

In a recent review Solomon and Hadt[155] covered several more recent results which extend the understanding of the geometric and electronic structure of the electron transfer (ET) active sites in the type 1 (T1) or blue Cu (BC) proteins. Spectroscopic methods combined with DFT and TD-DFT calculations have been used in studies of S → Se variants C112SeC and M121SeM of *Pseudomonas aeruginosa* azurin (Az) as well as a series of metal-varied model complexes ($M = Mn^{2+} \rightarrow Zn^{2+}$) in order to quantitatively evaluate the effects of replacing the S(Met) and S(Cys) with Se(Met) and Se(Cys), respectively. The conserved ligand set, S(Cys), S(Met), and 2N(His), gives rise to spectral features and properties due to protein constraints which derive from first coordination sphere effects. These unique spectral features show different temperature dependencies in different T1 sites. The contrasts drawn between their behaviors define the role of the protein in tuning the geometric and electronic structure of the BC site for function. The constraints necessary to oppose the entropy increase and prohibit Cu–S(Met) bond dissociation at physiological temperatures

(Scheme 9) has been termed the "entatic" or "rack-induced" state in BC proteins.

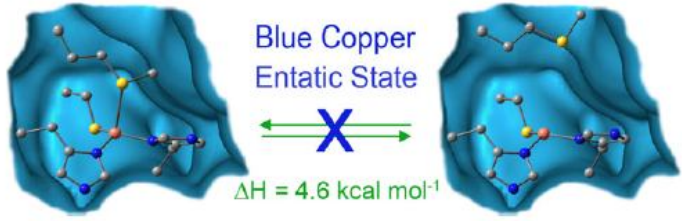

Scheme 9 Graphical representation of the "entatic" or "rank-induced" state in T1 BC proteins (reproduced with permission from ref. 155).

To gain insight into the chemistry in the active sites of mononuclear copper monooxygenases, the structures, properties and reactivity of copper(I) and copper(II) complexes supported by a series of tridentate ligands having the same *N*-[2-(2-pyridyl)ethyl]-1,5-diazacyclooctane framework have been examined in detail by means of experimental and DFT methods.[156] The ligand exhibits unique feature to stabilize the copper(I) complexes in a T-shape geometry and the copper(II) complexes in a distorted tetrahedral geometry. DFT (M11-L) calculations indicated that mononuclear copper(II) end-on superoxo complexes, generated from the low temperature oxygenation of the copper(I) complexes, having a four-coordinate distorted tetrahedral geometry could be reactive enough to induce the direct C−H bond activation of aliphatic substrates in the enzymatic systems. At low copper concentrations, C−H bond abstraction proceeds unimolecularly from the superoxo complex with subsequent rebound of the copper hydroperoxo species to generate an oxygenated ligand.

The tight-binding approximation of DFT (DFTB) was employed for the study of speciation of metal−peptide complexes in water solution.[157] The DFTB and DFT methods were applied to the study of different forms of the [Cu(HGGG)(Py)] (H = histidine, G = glycine, Py = pyridine) complex in water. It was concluded that in the presence of pyridine the lowest energy isomer is the five coordinated form $CuN_HN_{G1}N_{G2}O_{G2}N_{Py}$. The speciation process was carried out by computing different DFTB-steered molecular dynamics (SMD) trajectories, each of which ends in a well-defined different form. The last frame of each trajectory is subjected to geometry optimization at both DFTB and DFT levels, leading to a different isomer. From the corresponding energy values, a rank of relative stability of the isomers was established. The computational protocol was found to be of general applicability to other metal−peptide systems and represents a new powerful tool for the study of speciation of metal-containing systems in water solution, particularly useful when the full characterization of the compound cannot be carried out on the basis of experimental results only.

Miličević and Raos[158] compared the DFT and the method with the molecular valence connectivity index of the 3rd order ($^3\chi^v$) in the estimation of stability constants log β_2, of copper(II) complexes with thioflavin-based intercalation compounds designed for application in Alzheimer's disease (AD). It was shown that $^3\chi^v$ correlates to the log β_2 of the Cu(II) complexes much better than metalloaromaticity indices I_{NG} and HOMA. Considering the role of metal ions in AD, a promising therapeutic treatment could be based on metal ion chelation.

Accordingly, Sodupe and co-workers[159] studied the coordinative properties of a set of chelating ligands toward Cu(II) by means of DFT(B3LYP) calculations. Special attention has been paid to the aromatic behavior of the metalated rings of the complex and its influence on the chelating ability of the ligand. Calculations indicated that there is a good correlation between the stability constants ($\log \beta_2$) and the degree of metalloaromaticity determined through the I_{NG} and HOMA indices. Detailed analysis of the nature of the Cu(II)-ligand bonding, performed through EDA calculations, indicated that ligands with less aromatic moieties have the negative charge more localized in the metalated ring.

Quintanar et al.[160] provided a general overview of the different Cu(II) binding sites in a cellular prion protein (PrP^C) and their redox properties, highlighting the contributions from electronic structure calculations and molecular dynamics simulations. Particular emphasis was placed in discussing the electronic structure of each Cu binding mode, as it is intimately related to redox properties. For most Cu binding modes, the dominating Cu(II) bonding interactions involve deprotonated amide nitrogens, which yield Cu-Namide bonds that are significantly more covalent than the Cu-NHis bond. The impact of Cu–PrP^C interactions in the protein structure and the molecular mechanisms that may initiate PrP^C aggregation were also discussed. Further advancements in the field are related with answering the question of how do Cu–PrP^C interactions relate to the physiological function of PrP^C and/or to protein aggregation and the molecular events producing disease? Answering this question requires further understanding on how Cu–PrP^C interactions are related to or modulated by other events, such as the presence and trafficking of other metal ions in neurons; and the interaction of Cu and PrPC with other membrane bound proteins and receptors.

The influence of the structure on the antioxidant activity of a series of Schiff bases and their copper(II) complexes as well as possible mechanisms of antioxidant activity were investigated by DFT calculations.[161] Calculated quantum-chemical descriptors provided insight to the reaction mechanism of the scavenging/antioxidant activity of tetradentate Schiff bases and their copper(II) complexes and two different reaction mechanisms were proposed. Dipole moment, bond dissociation energy, charge on oxygen atoms and charge on hydrogen atoms on N7 and N10 show high correlation with antioxidant activity of the investigated Schiff bases. 2,2′-diphenyl-1-picrylhydrazyl (DPPH) assay, one of the most important methods used for evaluation of antioxidant activity, may be neutralized either by direct reduction via electron-transfer or by radical quenching via hydrogen atom transfer. The H-atom transfer mechanism was defined as the most important for the antioxidant activity of the investigated Schiff bases while the proposed mechanism for the complexes was single electron transfer.

The acid-base and coordination properties of a family of pseudopeptidic ligands with C_2 symmetry derived from valine (Scheme 10) have been studied using a variety of techniques as a model for metal coordination in peptides and proteins.[162]

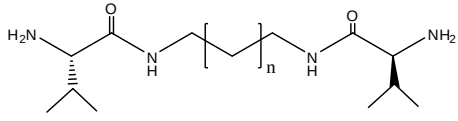

n = 0-4

Scheme 10 Pseudopeptidic ligands derived from valine.

These pseudopeptidic ligands form complexes of very different structures with metal ions such as Cu^{2+} and Zn^{2+}. The complex formation was analyzed by a combination of pH-metric titrations, spectroscopic studies, and ESI-MS experiments. Two critical factors determining the final structure are the nature of the aliphatic spacer connecting the amino acid subunits and the pH value at which the complex is formed. García-España's group[163] reported also the synthesis of two ligands constituted of a tris(2-aminoethyl)amine moiety linked to the 2,6 positions of a pyridine spacer through methylene groups in which the hanging arm is further functionalized with a 2-pycolyl (L1) or 3-pycolyl (L2) group. The protonation of L1 and L2 and formation of Cu^{2+} complexes have been studied using potentiometric, NMR, X-ray, and kinetic experiments. The results provided new information about the relevance of molecular movements in the chemistry of Cu^{2+} with this kind of so-called scorpiand ligand. DFT calculations provided a full picture of the mechanistic pathway leading to the formation of the first Cu-N bond through outer-sphere complexation followed by water dissociation to yield new outer-sphere complexes with the geometries adequate for evolving to inner-sphere metal complexes. In a more recent publication García-España and co-workers[164] reported the results of potentiometric studies of the formation of mono-, bi- and trinuclear Cu^{2+} complexes with two tritopic double-scorpiand receptors in which two equivalent 5-(2-aminoethyl)-2,5,8-triaza[9]-(2,6)-pyridinophane moieties are linked with 2,9-dimethylphenanthroline (L1) and 2,6-dimethylpyridine (L2). Kinetic experiments provided information about the movement of the metal ion within the receptors. In a similar vein a family of ligands derived from bis(amino amides) containing aliphatic spacers has been prepared, and their protonation and stability constants for the formation of Cu^{2+} complexes have been determined potentiometrically.[165] DFT calculations revealed the existence of different geometries in this kind of copper(II) complexes. In particular, for the complexes formed by bis deprotonated ligands containing shorter spacers, the square planar complex and square pyramidal seem to coexist.

2.5. TDDFT insights on the photophysics of copper coordination compounds

Computation of the spectroscopic and photochemical properties of transition metal complexes is of paramount importance to optimize their performance as light harvesting antennae or photocatalytic centers in photochemical devices, as sensitizers of solar energy conversion, phosphorescent dyes for display applications (organic light emitting diodes, OLED), luminescence-based sensors, active components of electron- or energy-transfer assemblies, molecular devices (molectronics), non-linear optical materials, photoinitiators, triggers of electron transfer in biomolecules, or photocatalysts, providing useful hints to guide molecular design strategies.

Electronic structure calculations of excited states of transition metal complexes have become nowadays a very important complement to spectroscopic techniques. However, the study of ground and excited state properties of coordination compounds using computational methods confront some difficulties arising from the size, the state degeneracies, the dynamical correlation and relativistic effects. Although the most appropriate formalism to describe the ground state and excited state properties of coordination compounds seems to be the multi-configurational (MCSCF) one including relativistic effects, nowadays TDDFT methods are

extensively used to simulate the electronic spectra of transition metal complexes. An overview of recent progress on TD-DFT with a specific focus on its accuracy and on models able to take into account environmental effects, including complex media was presented by Jacquemin and co-workers.[166] Very recently Laurent and Jacquemin[167] reviewed contributions devoted to the assessment of the performances of exchange-correlation DFs within TD-DFT framework. Garino and Salassa[168] presented an overview on photochemically active transition metal complexes investigated by TD-DFT.

Cu(I) complexes and clusters are the largest class of compounds of relevant photochemical and photophysical interest. A scholarly and authoritative survey of photochemistry and photophysics of copper coordination compounds by Armaroli et al.[169] is very informative. Well-established synthetic protocols are available to build up a variety of molecular and supramolecular architectures containing Cu(I)-based centers and exhibiting photo- and electroluminescence as well as light-induced intercomponent processes. The photophysics of Cu(I) complexes has attracted increasing attention for technological applications (e.g. OLEDs) and, although it is still at the level of prototypes and proofs of principles, further important breakthroughs may be anticipated in the years to come.

The largest class of copper complexes investigated to date is that of Cu(I)-bisphenanthrolines ($[Cu(N\hat{}N)_2]^+$) (N^N = phenanthroline). The molecular structure and dynamics of the photoexcited metal-to-ligand-charge-transfer (MLCT) state of $[Cu^I(dmp)_2]^+$ (dmp = 2,9-dimethyl-1,10-phenanthroline) in acetonitrile have been investigated by time-domain pump-probe X-ray absorption spectroscopy, femtosecond optical transient spectroscopy, and DFT.[170] DFT calculations were used to interpret the spectral shift on structural relaxation and to predict the geometries of the ground state, the tetracoordinate excited state, and the exciplex. The variation of the MLCT state structure in different solvents confirmed that the origin of distinctly different excited state behavior is due to formation of MLCT state-solvent complexes with different electronic interactions. The photophysical properties of singlet and triplet MLCT states of $[Cu^I(diimine)_2]^+$ (diimine = 2,9-dimethyl-1,10-phenanthroline (dmphen), 2,9-dibutyl-1,10-phenanthroline (dbphen), or 6,6′-dimethyl-2,2′-bipyridine (dmbpy), were studied by experimental and DFT methods.[171] Scheme 11 summarizes the photophysical properties of the MLCT states of $[Cu(dmphen)_2]^+$ in CH_2Cl_2 that illustrate the comparisons between the observed and the calculated values (in parentheses) based on the information obtained from DFT. DFT calculations revealed that the inter system crossing (ISC) channels induced by large spin-orbit interaction (ca. 300 cm^{-1}) between the metal-centered HOMO and HOMO-1 were energetically unfavorable in the copper(I) compounds because the flattening distortion caused large splitting (6.9×10^3 cm^{-1}) between these orbitals, considerably decreasing the Franck-Condon-weighted density of the final vibronic states (FCWDs) of these channels. The DFT calculations also revealed that the structure of the lowest ^{1}MLCT in $[Cu(dmphen)_2]^+$ (1^1B_1) was flattened due to the Jahn-Teller effect in $3d^9$ electron configuration, and the dihedral angle between the two phenanthroline planes (dha) was about 75° with the dha around 90° in the ground state. Intramolecular reorganization energy for the radiative transition of 1^1B_1 was calculated as 2.1×10^3 cm^{-1}, which is responsible for the large Stokes shift of the fluorescence observed (5.4×10^3 cm^{-1}).

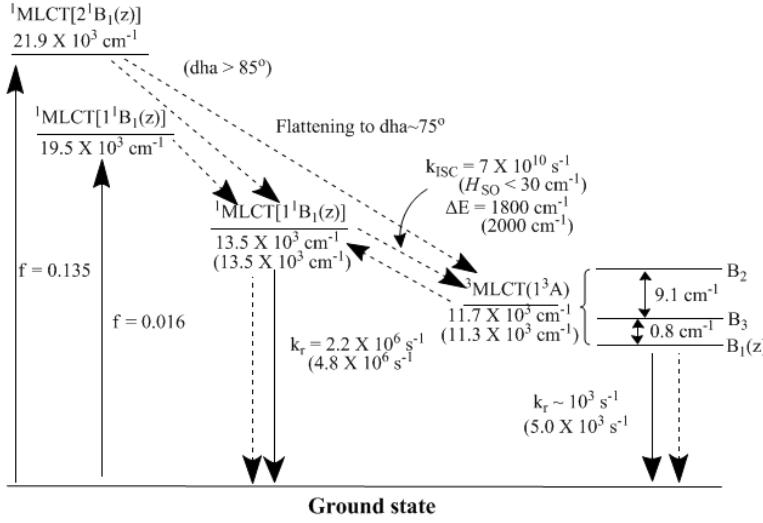

[a] Calcd values are in parentheses.

Scheme 11 Comparison between the observed and calculated properties of MLCT states of $[Cu(dmphen)_2]^+$ in CH_2Cl_2 (reproduced with permission from ref. 171).

The charge transfer and structural distortions that occurred in the bis-phenanthroline $[Cu(N\text{^}N)_2]^+$ (N^N denotes 1,10-phenanthroline, 2,9-dimethyl-1,10-phenanthroline and 2,9-di(trifluoromethyl)-1,10-phenanthroline) copper(I) complexes upon excitation with an irradiation of light were studied by DFT.[172] The calculations showed that the electrons transferred from Cu(I) to ligands with the transition of the complexes $[Cu(N\text{^}N)_2]^+$ from ground state to excited state. After the Cu(I) complex captured the light energy, the electrons were redistributed by electronic transfer from the central metal to the ligands in forming a Cu(II)-like excited state. Accompanying with this transfer process, the coordination polyhedra of $[Cu(N\text{^}N)_2]^+$ became distorted upon excitation. The structural distortion was significantly reduced by increasing the steric bulk of the 2- and 9-positions substituents in the N^N ligands, which is helpful for the increase of the life time of the excited state. The decrease in structural distortion (ΔQ_e) reduced the amount of vibrational overlap between ground state and excited state, leading to smaller non-radiative decay rate constants and hence the extended lifetime of excited state.

DFT calculations employing the PBE0 density functional were performed to study the electronic structures of the ground and excited states of the luminescent tetranuclear copper(I) complexes $[Cu_4(\mu\text{-dppm})_4(\mu_4\text{-E})]^{2+}$ (E = PPh or S) by using the $[Cu_4(\mu\text{-}H_2PCH_2PH_2)_4(\mu_4\text{-E})]^{2+}$model complexes.[173] The TDDFT calculations at the same level of theory associated with the conductor-like polarizable continuum model (CPCM) indicated that the lowest energy absorptions of both model complexes are attributed mainly to the LMCT (E → Cu_4)/MCC (3d → 4s/3d → 4p) singlet-singlet transitions (MCC refers to metal-cluster-centered transitions). The geometry optimizations on the lowest energy triplet state revealed that the emissive states of both complexes involve a considerable structural distortion in which they are derived predominantly from an admixture of ^{3}LMCT (E → Cu_4) and ^{3}MCC (3d → 4p) origin.

An overview of the photophysical behaviour of copper phenanthroline complexes was presented by McClenaghan and co-workers,[174] with an emphasis on recent developments and insights, as well as ramifications for developing successful strategies to prolong luminescence lifetimes and increase quantum yields.

The optical properties of the trinuclear {[3,5-$(CF_3)_2$Pz]Cu}$_3$ in monomeric and dimeric forms were explored by theoretical approaches based on DFT.[175] TD-DFT calculations employing various DFs (BPW91, B3PW91, BP86, B3P86, BLYP, B3LYP, and SVWN5) indicated that the emission of all complexes originates from T_1, and the corresponding emissive states are assigned as ^{3}MCCT/^{3}LMCT. Calculations also suggest that the shortest intermolecular Cu···Cu distance plays an important role in the emission spectra of the vertical and tilting-movement dimers, which is ascribed to the variation of the energy gap for the frontier molecular orbitals involved in the main emitting transition. The blue shift of λ_{em} in parallel-movement and rotational dimers can be attributed to the variation of the mutual spatial orientation. Therefore, the modulation of the extent of movement or rotational angles for stacked dimers by external perturbations creates new possibilities for the design of molecular light-emitting devices.

The structural, spectroscopic (luminescent), bonding and electronic properties of some mixed-ligand copper(I) complexes formulated as [Cu(κ^3-triphos)(thiolate)], were explored using both experimental and computational (DFT and TD-DFT) methodologies in conjunction with single crystal X-ray studies.[176] The relationship between structure and luminescence and evaluation of the impact of the thiolate ligand on the luminescence properties of the new copper(I) complexes was also explored. The intense blue-green emission found in the 456–502 nm range of the emission spectra is due to a $T_1 \rightarrow S_0$ transition corresponding to a distant interligand charge transfer (LLCT) mediated by the copper central metal atom.

Holland and Green[177] evaluated the relative and absolute performance of a wide range of XC functionals in TD-DFT calculations of UV/vis spectra of a range of copper and zinc complexes (Scheme 12).

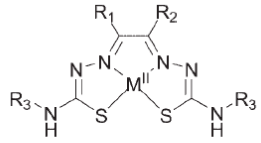

Complex	R_1	R_2	R_3
1 [Cu^{II}ATSM]	Me	Me	Me
2 [Zn^{II}ATSM]	Me	Me	Me
3 [Cu^{II}GTS]	H	H	H
4 [Cu^{II}PTS]	Me	H	H

Scheme 12 Structures of the copper and zinc bis(thiosemicarbazonato) complexes used for TD-DFT functional testing (reproduced with permission from ref. 177).

The results indicated that hybrid functionals provide the best description of the electronic excited state transitions (both ω_I and f_I values) but larger variations are observed depending on the system studied. B1LYP, B97-2, and B97-1 gave consistently high performance irrespective of the electronic configuration (closed or open shell) and structure. Of the density functionals tested, B1LYP gave the most

accurate results with both average root-mean-squared errors (RMSE) quality-of-fit (Q_F) parameters and overall energy scaling factors ($e_{SF)}$ values close to unity (>0.990) for the copper complexes.

DFT and TD-DFT calculations were employed to study the structural, electronic and photophysical properties of heteroleptic copper(I) halide complexes containing the bis[2-(diphenylphosphano)phenyl]ether (DPEphos) ligand and the heterocyclic thioamides pyridine-2(1H)-thione (py2SH), pyrimidine-2(1H)-thione (pymtH) or 4,6-dimethylpyrimidine-2(1H)-thione (dmpymtH) ligands.[178] The electronic absorption spectra of these complexes show two broad bands in the regions 275–290 and 380–398 nm, which according to TD-DFT calculations were assigned as having MLL′CT/IL character. An intense blue–green emission in the range 500–558 nm is observed for complexes of py2SH or dmpymtH thione ligands, while complexes of the pymtH ligand show only weak emission. However, based upon the TD-DFT simulated emission spectra both in the gas phase and in CH_2Cl_2 solution, it is expected to have additional emission bands in the UV-Vis and near-IR regions. The largest $\Delta E_{T_1\text{-}S_0}$ energy gap amongst all complexes under investigation is found for the complexes with pymtH ligand and therefore it is expected that they would have the smallest nonradiative decay rate constant, k_{nr}.

Alemayehu et al.[179] carried out the first TDDFT analysis of a series of metallotriarylcorrole (Fig. 5) derivatives with *meso*-triarylcorroles with varying *para* substituents on the *meso* phenyl groups, symbolized M[T(*p*-X-P)C], where M = Cu and Ag and X = CF_3, H, CH_3, and OCH_3. TDDFT calculations indicated that the substituent sensitivity in the copper triarylcorroles results from significant phenyl-to-metal charge-transfer character in the main peaks of the Soret region. Copper exhibit so-called hyper spectra; the Soret band includes one or more transitions with substantial phenyl-to-metal charge-transfer character. The TDDFT calculations reproduced the Soret red shift of Cu[T(*p*-CH_3-P)C] relative to that for Cu(TPC).

The solvent effects on the optical and magnetic spectra of Cu(II) acetylacetonate (acac) complex have been investigated by DFT methods.[180] Calculations have been performed using the supermolecule model to describe the direct solvent interactions with the $Cu(acac)_2$ complex. The visible near-infrared absorption transitions showed a strong dependence on the coordination environment around the copper complex. High solvatocromic shifts are observed for $3d \rightarrow 3d$ transitions, with the highest effect observed for the $d_z^2 \rightarrow d_{xy}$ transition, which is red-shifted by 6000 cm^{-1} and 9000 cm^{-1} in water and pyridine solvent models, respectively. The estimated $3d \rightarrow 3d$ excitation energies employing the B3LYP functional show that each model of the solvated model complex gives rise to a particular spectral pattern of the absorption spectrum, where both positions and intensities of electronic transitions can be used to characterize the coordination environment of the first solvation shell around the $Cu(acac)_2$ complex in solution. The good comparison with experimental results indicates that the coordination of the solvent at axial position of $Cu(acac)_2$ should indeed be the main solvent effect on the positions and intensities of absorption bands in $Cu(acac)_2$.

The electronic structures and photophysical properties of Cu(I) complexes with phenathroline ligands, which are substituted in the 2,9-positions with methyl, phenyl, trifluoromethyl and tert-butyl groups (Scheme 13), has been studied by DFT and TDDFT computational methods.[181]

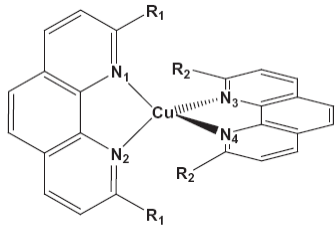

$R_1 = R_2 = H$, $[Cu(Phen)_2]^+$
$R_1 = R_2 = CH_3$, $[Cu(dmp)_2]^+$
$R_1 = R_2 = Ph$, $[Cu(dpp)_2]^+$
$R_1 = R_2 = CF_3$, $[Cu(bfp)_2]^+$
$R_1 = CH_3$, $R_2 =$ t-Bu, $[Cu(dtbp)(dmp)]^+$

Scheme 13 Sketch map of the studied structures (reproduced with permission from ref. 181).

The calculated eigenvalues of HOMO and LUMO, the HOMO-LUMO energy gap, $\Delta\varepsilon_{H-}\varepsilon_L$, the lowest excitation energies (E_{S_1}), the ionization potentials (IPs), the electron affinities (EAs) and reorganization energies (k) revealed that the ability of the hole injection is dramatically improved with the presence of counteranion. The hole transport rate is condition of the transport equilibrium property in these complexes, regardless of with or without the presence of counterion. It was also concluded that the $[Cu(dtbp)(dmp)]^+$ complex has faster k_r and ISC, but slower k_{nr}, which leads to its highest photoluminescent quantum efficiency among the studied complexes. Moreover, the $[Cu(dtbp)(dmp)]^+$ has smaller dihedral angles (DHAs) and stokes shift than others, owing to the t-butyl group, which dramatically prevents the flattening distortion of the copper complex.

A new series of Cu(I) heteroleptic complexes $[CuL_1L_2]^+$ (L_1 = phen-imidazole and/or L_2 = dipyrido [3,2-a:2′,3′-c] phenazine derivatives) has been investigated theoretically by means of DFT/TD-DFT calculations with DFT-D functionals for the structural investigation and B3LYP for excited states determination.[182] The geometries of the ground states, characterized by π-stacking interactions, have been optimized using PBE-D functional. The UV-visible absorption spectra have been σιμθλατεδ using B3LYP functional in vacuum and taking into account solvent corrections by means of the PCM solvation model. The theoretical absorption spectra are characterized by high density of states of mixed character. Most of the transitions correspond to charge transfer towards L_1 with important contributions of MLCT states.

The structural, electronic, and optical properties of $[Cu_2(dbdmed)_2O_2]^{2+}$ and $[Cu_2(en)_2O_2]^{2+}$ have been calculated by Rohrmüller et al.[183] employing DFT and TDDFT methods. The ground state of the oxo (O) structure prefers the spin singlet, while the spin state of the peroxo (P) core depends on the specific exchange-correlation functional used in the calculations. In particular, hybrid functionals tend to favor the singlet state less than (semi)local functionals compared to the triplet. The results from occupation-constrained as well as ΔSCF and TDDFT calculations are compared with Green's function-based approaches within many-body perturbation theory such as the GW approximation (GWA) to the quasi-particle (QP) energies and the Bethe-Salpeter equation (BSE) approach to the optical absorption. Irrespective of whether they are calculated from the G_0W_0 approach or using

occupation constrained DFT, a value of about 5 eV marks the lower limit of the QP gap for both $[Cu_2(dbdmed)_2O_2]^{2+}$ and $[Cu_2(en)_2O_2]^{2+}$ complexes. In comparison to the single-particle gaps calculated within DFT-PW91, this corresponds to electronic self-energy effects of the order of about 4 eV. The semilocal DFs, such as PW91, predict larger QP gaps for P than for O, while the trend is reversed for calculations based on hybrid functionals. TDDFT calculations and the Bethe-Salpeter approach lead thereby to qualitatively similar spectra for $[Cu_2(en)_2O_2]^{2+}$ complex. In the case of $[Cu_2(dbdmed)_2O_2]^{2+}$ where measured optical absorption data are available, it was found that the TDDFT calculations describe the essential features of the experiment correctly but show a large scatter with respect to the influence of the basis set and the XC functional used in the adiabatic approximation. The agreement with experiment is best if B3LYP and CAM-B3LYP in conjunction with a 6-31G(d) basis set are used for O and P, respectively.

The photophysical properties of four new halide-bridged Cu(I) dimers with chelating aminophosphane ligands Ph_2P-(o-C_6H_4)- $N(CH_3)_2$ ($PNMe_2$) and Ph_2P-(o-C_6H_4)-NC_4H_8 (PNpy) were studied in detail by means of DFT and TDDFT calculations.[184] At ambient temperature, the complexes exhibit high photoluminescence quantum yields (up to 65%) and relatively short emission decay times (down to about 4 µs), and the emission color can be tuned from green to blue by variation of the halide X (X = Cl, Br, I). The involved electronic transitions are assigned to (metal + halide)-to-ligand CT character. Accordingly, the lowest excited singlet (S_1) and triplet (T_1) states are designated as ^{1,3}(M+X)LCT states. The drastic decrease of the (radiative) decay time observed is a result of the thermal population of a short-lived singlet state (S_1 state) that lies energetically only a few hundred wavenumbers (460−630 cm^{-1}) higher than the T_1 state. Such an emission mechanism depicted schematically in Fig. 7 corresponds to a thermally activated delayed fluorescence (TADF).

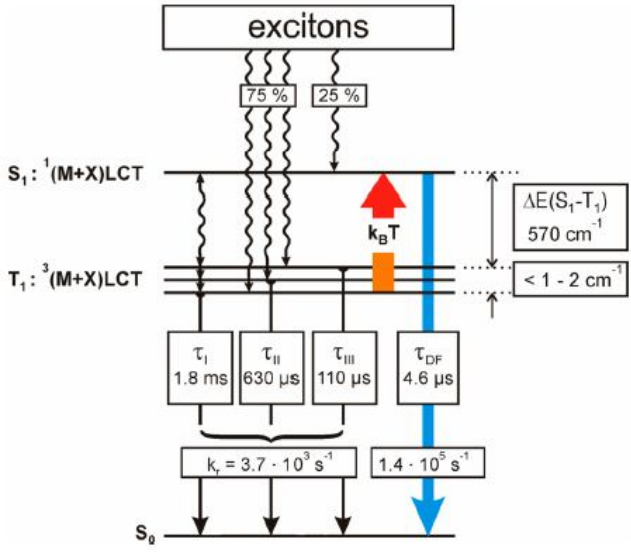

Fig. 7 Energy level diagram and decay times for $[Cu(\mu\text{-}I)(PNMe_2)]_2$ (reproduced with permission from ref. 184).

It can be seen that at a temperature below T ≈ 60 K, only a $T_1 \rightarrow S_0$ phosphorescence is observed. The T_1 state consists of three individual triplet substates I, II, and III. The corresponding decay times have been determined at T = 1.3 K. The calculated averaged value corresponds well to the measured decay time of the triplet state T_1 of $\tau(T_1)$ = 290 µs. The diagram displays also the (radiative) rates for the triplet state emission (calculated from the individual decay times as given in the diagram). With a temperature increase, the S_1 state is increasingly populated. As a consequence, the emission represents almost completely a TADF at ambient temperature with a decay time of τ(DF) = 6.6 µs. This effect can be applied in an OLED device to harvest all excitons for an emission that stems from the singlet state, and hence, singlet harvesting becomes effective. Interestingly, an emitter showing efficient TADF is highly attractive for OLED applications because all singlet (25%) and all triplet (75%) excitons that are generated in the emitter layer and trapped by the emitter molecule can, at least in principle, be harvested. At ambient temperature, almost only a delayed fluorescence (98%) is observed.

An extensive DFT and TDDFT study of copper complexes with bipyridine ligands and carboxylic acid or methyl ester as anchoring groups (Scheme 14) was performed, investigating the electronic structures and optical properties of the complexes in solution.[185] The DFT and TDDFT calculations were performed using M06 hybrid-meta-GGA functional combined with the LANL2DZ and DZVP basis sets. The complexes under study showed UV–vis absorptions in the 590–690 nm range. For all complexes molecular orbitals energy levels meet the requirements for use in dye sensitized solar cells (DSSCs).

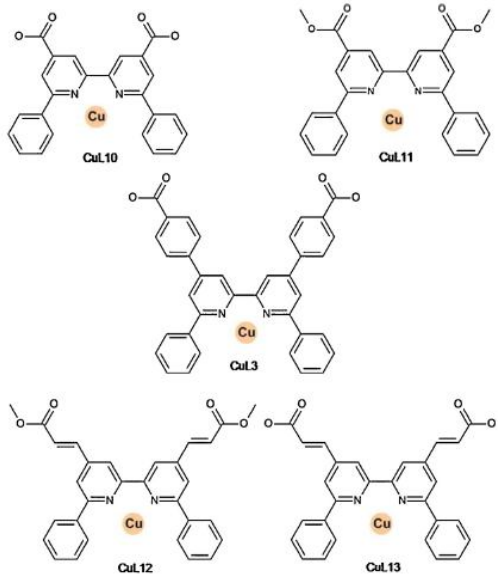

Scheme 14 Molecular structure of bipyridine ligands for copper complexes (reproduced with permission from ref. 185).

The structural features and photophysical properties of a new series of luminescent monometallic Cu(I) complexes with functionalized 3-(2′-pyridyl)-1,2,4-triazole

ligands (Scheme 15) have been fully investigated by Chen and co-workers.[186] All these complexes show a relatively weak low-energy absorption in CH_2Cl_2 solution. According to TD-DFT calculations using the PBE0 DF the low-energy absorption is ascribed to the charge-transfer transitions with appreciable MLCT character. Complexes **5**–**9** have good luminescence properties in degassed CH_2Cl_2 solution, despite the halide complexes **1**–**4** being nonemissive in fluid solution. These results might provide new insight into the synthesis of blue phosphorescent materials of the 3-(2′-pyridyl)-1,2,4-triazole-based copper(I) complexes with potentially high luminescence efficiency.

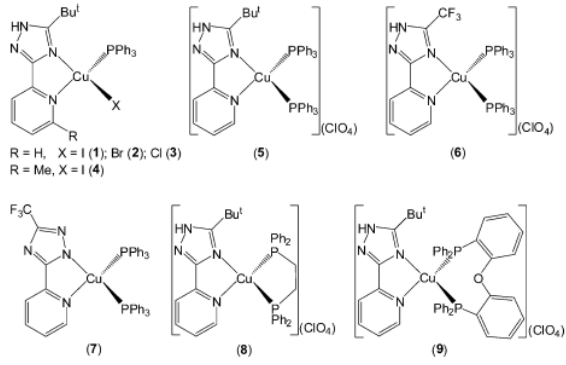

Scheme 15 Molecular structure of bipyridine ligands for copper complexes (reproduced with permission from ref. 186).

Very recently Ziegler and co-workers[187] presented a comparative study of three different DFT methods (TDDFT/TDA, DDFT, and DSCF-DFT) and five different functionals (LDA, BP86, B3LYP, PBE0, and LC-BP86 with $\gamma = 0.4$) for evaluation of excitation energies in a D_{2d} model of $CuCl_4^{2-}$ and a model of the blue copper site derived from the crystal structure of plastocyanin (Scheme 16).

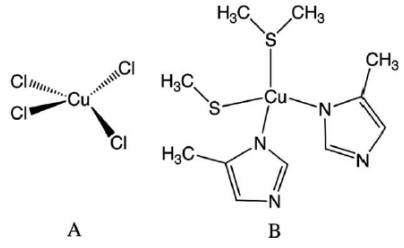

Scheme 16 Models used in the calculations: A) D_{2d}–symmetrized $CuCl_4^{2-}$. B) Plastocyanin (reproduced with permission from ref. 187).

Some well-known deficiencies observed in TDDFT were explained on the basis of lacking orbital relaxation and two-electron terms not considered in adiabatic TDDFT. Δself consistent field (SCF)-DFT (ΔSCF-DFT) reproduces well the position of the charge-transfer excitations and yields results in best agreement with experiment regardless of the system or functional used. The authors concluded that the orbital relaxation and proper account of higher-order terms neglected in adiabatic TDDFT are of great importance for the simulation of excitation spectra.

Karlin et al.[188] reported the first example of a photodissociation of molecular oxygen from cupric−superoxide complexes (Scheme 17).

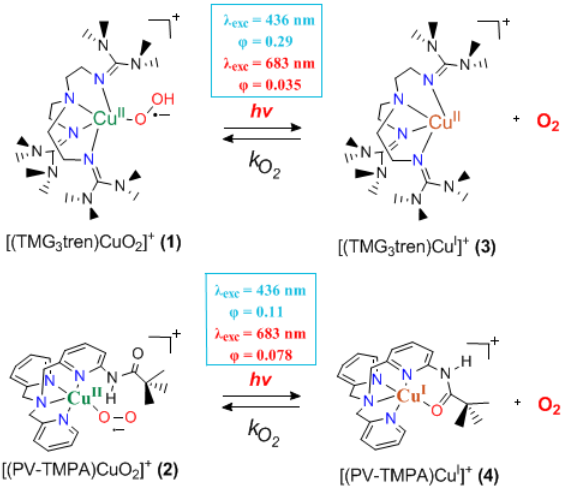

Scheme 17 (reproduced with permission from ref. 188).

Laser excitation either into the LMCT band, using 436 nm light, or into the d−d electronic transition, using 683 nm light induce copper−oxygen bond breaking in $[(TMG_3tren)Cu^{II}(O_2)]^+$ and $[(PV\text{-}TMPA)Cu^{II}(O_2)]^+$. Interestingly, the quantum yield for O_2 release was wavelength dependent. TD-DFT studies elucidated the O_2 photorelease event occurring upon irradiation with red light on the basis of (a) population of a molecular orbital ($3d_{z^2}$) that has strong σ-antibonding character along the Cu−O bond and (b) energy surface crossing between the d−d and the LMCT excited states to lead to O_2 release. These findings add new insights into the observed wavelength dependent Cu/O_2 photochemistry which differs markedly from that observed with hemes.

3 Conclusions

Density functional theory (DFT) and time-dependent DFT (TDDFT) have nowadays become general tools to the understanding and predicting the behavior of a broad range of chemical, physical, and biological phenomena featuring the realm of copper coordination chemistry. DFT is less demanding than other computational methods with similar accuracy; and permits the study of molecular systems containing up to 200 atoms, a feature that is not yet feasible with high accuracy methods such as CCSD(T) or even second order Möller-Plesset perturbation theory (MP2).

Copper compounds have found a widespread use in a range of applications in catalysis, medicinal chemistry and applied material sciences relating to electron transport devices and organic light-emitting diodes (OLEDs). DFT and TDDFT have been growing as excellent alternatives and complementary methodologies to the common experimental procedures used to study metalloproteins and a great diversity of copper coordination compounds. However, in the case of the copper coordination compounds, the experimental spectroscopic methodologies, such as EPR, ENDOR, ESEEM, NMR, IR and Raman, ABS, CD, XAS, and EXAFS, are often not enough

to fully characterize such complexes, and so, DFT methods have arisen as an excellent complement to their characterization. This is supported by the numerous theoretical studies that surfaced in the literature over the years, the most recent ones presented herein.

Application of the DFT and TDDFT methods in copper coordination chemistry could provide insights on:

(i) the bonding mechanisms in copper coordination compounds.

(ii) the mechanisms of a diverse array of copper-catalyzed reactions, that help experimentalists to generate of more efficient and selective, eco-friendly, copper-based catalysts for applications with industrial relevance.

(iii) the bioactivity of copper coordination compounds and copper-containing enzymes that help to design and produce novel copper-based anticancer drugs to improve clinical effectiveness, to reduce general toxicity, and to broaden the spectrum of activity.

(iv) the photophysical properties of copper coordination compounds exhibiting broad interest to potential applications in various fields, such as organic light-emitting diodes (OLEDs), light-emitting electrochemical cells (LECs), supramolecular assemblies, chemical sensors, solar-energy conversion schemes, dye sensitized solar cells, biological probing and oxygen sensing.

References

[a] *Laboratory of Inorganic and General Chemistry, Department of Chemistry, University of Ioannina, 451 10 Ioannina, Greece, Fax: XX XXXX XXXX; Tel: XX XXXX XXXX; E-mail: attsipis@uoi.gr*

1 S. H. Bertz, S. Cope, M. Murphy, C. A. Ogle and B. J. Taylor, *J. Am. Chem. Soc.*, 2007, **129**, 7208.

2 B. J. Hathaway, In *Comprehensive Coordination Chemistry*, G. Wilkinson, R. D. Gillard and J. A. McCleverty, Eds., Pergamon Press: Oxford (UK), 1987; Vol. **5**, 533.

3 R. Mukherjee, Copper. In *Comprehensive Coordination Chemistry II - From Biology to Nanotechnology*, J. A. McCleverty and T. J. Meyer, Eds., Elsevier Ltd.; Oxford (UK), 2004; Vol. **6**, 747.

4 N. Krause, *Modern Organocopper Chemistry*; Wiley-VCH: Weinheim, Germany, 2002.

5 J. Hassan, M. Sevignon, C. Gozzi, E. Schulz and M. Lemaire, *Chem. Rev.* 2002, **102**, 1359.

6 S. Trofimenko, In *Scorpionates: The Coordination Chemistry of Polypyrazolylborate Ligands*; Imperial College Press: London, 1999.

7 C. Pettinari, *Scorpionates II: Chelating Borate Ligands*; Imperial College Press: River Edge, NJ, 2008.

8 A. Conde, L. Vilella, D. Balcells, M. M. Díaz-Requejo, A. Lledós and P. J. Pérez, *J. Am. Chem. Soc.*, 2013, **135**, 3887.

9 K. Sonogashira, Y. Tohda and N. Hagihara, *Tetrahedron Lett.*, 1975, **16**, 4467.

10 L.-H. Zou, A. J. Johansson, E. Zuidema and C. Bolm, *Chem. Eur. J.* 2013, **19**, 8144.

11 R. Schmidt, R. Thorwirth, T. Szuppa, A. Stolle, B. Ondruschka and H. Hopf, *Chem. Eur. J.*, 2011, **17**, 8129.

12 X. Niu, C. Li, J. Li and X. Jia, *Tetrahedron Lett.*, 2012, **53**, 5559.

13 P. Beletskaya and A. V. Cheprakov, *Coord. Chem. Rev.*, 2004, **248**, 2337.

14 L. M. Stanley and M. P. Sibi, *Chem. Rev.*, 2008, **108**, 2887.

15 A. Alexakis, J. E. Backvall, N. Krause, O. Pamies and M. Dieguez, *Chem. Rev.*, 2008, **108**, 2796.

16 K. Yamada and K. Tomioka, *Chem. Rev.*, 2008, **108**, 2874.

17 S. Reymond and J. Cossy, *Chem. Rev.*, 2008, **108**, 5359.

18 T. Jerphagnon, M. G. Pizzuti, A. J. Minnaard and B. L. Feringa, *Chem. Soc. Rev.*, 2009, **38**, 1039.

19 J. E. Hein and V. V. Fokin, *Chem. Soc. Rev.*, 2010, **39**, 1302.

20 C. Zhang, C. Tang and N. Jiao, *Chem. Soc. Rev.*, 2012, **41**, 3464.
21 S. E. Allen, R. R. Walvoord, R. Padilla-Salinas and M. C. Kozlowski, *Chem. Rev.*, 2013, **113**, 6234.
22 T. Sugiishi, A. Kimura and H. Nakamura, *J. Am. Chem. Soc.*, 2010, **132**, 5332.
23 C. A. He, S. Guo, L. Huang and A. Lei, *J. Am. Chem. Soc.*, 2010, **132**, 8273.
24 W. Zhou, Y. Yang, Y. Liu and G.-J. Deng, *Green Chem.*, 2013, **15**, 76.
25 B.-X. Tang, R.-J. Song, C.-Y. Wu, Y. Liu, M.-B. Zhou, W.-T. Wei, G.-B. Deng, D.-L. Yin and J.-H. Li, *J. Am. Chem. Soc.*, 2010, **132**, 8900.
26 M. Nishino, K. Hirano, T. Satoh and M. Miura, *J. Org. Chem.*, 2011, **76**, 6447.
27 Z.-Q. Wang, W.-W. Zhang, L.-B. Gong, R.-Y. Tang, X.-H. Yang, Y. Liu and J.-H. Li, *Angew. Chem. Int. Ed.*, 2011, **50**, 8968.
28 G. Zhang, J. Miao, Y. Zhao and H. Ge, *Angew. Chem. Int. Ed.*, 2012, **51**, 8318.
29 C. W. Cheung and S. L. Buchwald, *J. Org. Chem.*, 2012, **77**, 7526.
30 Y. Li, Z. Li, T. Xiong, Q. Zhang and X. Zhang, *Org. Lett.*, 2012, **14**, 3522.
31 A. E. Wendlandt and S. S. Stahl, *Org. Biomol. Chem.*, 2012, **10**, 3866.
32 G. Zhang, Y. Zhao and H. Ge, *Angew. Chem. Int. Ed.*, 2013, **52**, 2559.
33 K. Kubota, E. Yamamoto and H. Ito, *J. Am. Chem. Soc.*, 2013, **135**, 2635.
34 S. Woodward, in *Copper-Catalyzed Asymmetric Synthesis*, A. Alexakis, N. Krause and S. Woodward, Eds., 2014 Wiley-VCH Verlag GmbH & Co. KGaA.
35 L. M. Mirica, X. Ottenwaelder and T. D. P. Stack, *Chem. Rev.*, 2004, **104**, 1013.
36 W. B. Tolman, *Acc. Chem. Res.*, 1997, **30**, 227.
37 D. M. Medeiros and D. J. Jennings, *Bioenerg. Biomembr.*, 2002, **34**, 389.
38 C. Marzano1, M. Pellei, F. Tisato and C. Santini, *Anti-Cancer Agents in Med. Chem.*, 2009, **9**, 185.
39 F. Tisato, C. Marzano, M. Porchia, M. Pellei and C. Santini, *Med. Res. Rev.*, 2010, **30**, 708.
40 I. Iakovidis, I. Delimaris and S. M. Piperakis, *Mol. Biol. Int*, 2011, 1.
41 R. F. Brissos, S. García, A. Presa and P. Gamez, *Comm. Inorg. Chem.*, 2011, **32**, 219.
42 W.L. Jia, T. McCormick, Y. Tao, J.P. Lu and S. Wang, *Inorg. Chem*. 2005, **44**, 5706.
43 S.M. Kuang, D.G. Cuttell, D.R. McMillin, P.E. Fanwick and R.A. Walton, *Inorg. Chem*. 2002, **41**, 3313.
44 Q.S. Zhang, Q.G. Zhou, Y.X. Cheng, L.X. Wang, D.G. Ma, X.B. Jing and F.S. Wang, *Adv. Mater*. 2004, **16**, 432.
45 W. Wei, M. Wu, Q. Gao, Q. Zhang, Y. Huang, F. Jiang and M. Hong, *Inorg. Chem*. 2009, **48**, 420.
46 S.B. Harkins and J.C. Peters, *J. Am. Chem. Soc*. 2005, **127**, 2030.
47 T. Besho, E.C. Constable, M. Graetzel, A.H. Redondo, C.E. Housecroft, W. Kylberg, M.K. Nazeeruddin, M. Neuburger and S. Schaffner, *Chem. Commun*. 2008, 3717.
48 A. Hernandez Rendondo, E. C. Constable and C. E. Housecroft, *Chimia*, 2009, **63**, 205.
49 M.T. Miller and T.B. Karpishin, *Sens. Actuators B. Chem.*, 1999, **61**, 222.
50 L. Shi, B. Li, S. Yue and D. Fan, *Sens. Actuators B. Chem*., 2009, **137**, 386.
51 F. Voges, K. Bonrad, T. K. Daubler, T. Frank, J. Pommerehne, C. Ottermann, and R. Sprengard, In *Light Sources 2004*; Zissis, G., Ed.; Iop Publishing Ltd: Bristol, 2004, 183.
52 T. N. Sorrell, A. S. Borovik and C. C. Chen, *Inorg. Chem*., 1986, **25**, 590.
53 V.W.W. Yam, K.K.W. Lo, W.K.M. Fung and C.R. Wang, *Coord. Chem. Rev*., 1998, **171**, 17.
54 P. Fernandez, A. Sousa-Pedrares, J. Romero, M. L. Duran, A. Sousa, P. Perez-Lourido and J. A. Garcia-Vazquez, *Eur. J. Inorg. Chem.*, 2010, **2010**, 814.
55 M. Spescha and G. Rihs, *Helvetica Chimica Acta* 1993, **76**, 1219.
56 I. G. Dance, P. J. Guerney, A. D. Rae and M. L. Scudder, *Inorg. Chem.* 1983, **22**, 2883.
57 P. C. Ford, E. Cariati and J. Bourassa, *Chem. Rev.* 1999, **99**, 3625.
58 D. V. Scaltrito, D. W. Thompson, J. A. O'Callaghan and G. J. Meyer, *Coord. Chem. Rev.* 2000, **208**, 243.
59 N. Armaroli, G. Accorsi, F. Cardinali and A. Listorti, A. In *Photochemistry and Photophysics of Coordination Compounds I* 2007; Vol. 280, 69.
60 N. Armaroli, A. Gianluca and F. Cardinali, *Top. Curr. Chem.*, 2007, **280**, 280.
61 K. J. Lotito and J. C. Peters, *Chem. Commun.*, 2010, **46**, 3690.
62 V. A. Krylova, P. I. Djurovich, M. T. Whited and M. E. Thompson, *Chem. Commun.*, 2010, **46**, 6696.
63 J. H. Min, Q. S. Zhang, W. Sun, Y. X. Cheng and L. X. Wang, *Dalton Trans.*, 2011, **40**, 686.

64 M. S. Lazorski and F. N. Castellano, *Polyhedron*, 2014, doi: http://dx.doi.org/10.1016/j.poly.2014.04.060
65 C.J. Cramer and D.G. Truhlar, *Phys. Chem. Chem. Phys.*, 2009, **11**, 10757.
66 A. C. Tsipis, Coord. Chem Rev., 2014, **272**, 1.
67 F. Neese, *Coord. Chem. Rev.*, 2009, **253**, 526.
68 K.P. Kepp, *Coord. Chem. Rev.*, 2013, **257**, 196.
69 S. F. Sousa, G. R. P. Pinto, A. J. M. Ribeiro, J. T. S. Coimbra, P. A. Fernandes and M. J. Ramos, *J. Comput. Chem.*, 2013, **34**, 2079.
70 A. Jesser, M. Rohrmüller, W. G. Schmidt and S. Herres-Pawlis, *J. Comput. Chem.*, 2014, **35**, 1.
71 T. Ansbacher, H. K. Srivastava, J. M. L. Martin and A. Shurki, *J. Comput. Chem.*, 2010, **31**, 75.
72 H. Schmidbaur, W. Graf and G. Müller, *Angew. Chem., Int. Ed. Engl.*, 1988, **27**, 417.
73 H. Schmidbaur, *Gold Bull.*, 1990, **23**, 11.
74 D. E. Harwell, M. D. Mortimer, C. B. Knobler, F. A. L. Anet and M. F. Hawthorne, *J. Am. Chem. Soc.*, 1996, **118**, 2679.
75 P. Pyykkö, *Chem. Rev.*, 1997, **97**, 597.
76 S. Dinda and A. G. Samuelson, *Chem. Eur. J.*, 2012, **18**, 3032.
77 R. F. W. Bader, *Atoms in Molecules, A Quantum Theory*, Oxford University Press, Oxford, 1990; R. F. W. Bader, *Chem. Rev.*, 1991, **91**, 893; R. F. W. Bader, *J. Phys. Chem. A*, 2007, **111**, 7966.
78 A. C. Tsipis and C. A. Tsipis, *J. Am. Chem. Soc.*, 2003, **125**, 1136.
79 P. v. R. Schleyer, C. Maerker, A. Dransfeld, H. Jao and N. v. E. Homes, *J. Am. Chem. Soc.* 1996, **118**, 6317.
80 S.-D. Li, G.-M. Ren, C.-Q. Miao and Z.-H. Jin, *Angew. Chem. Int. Ed.*, 2004, **43**, 1371.
81 S.-D. Li, C.-Q. Miao, and G.-M. Ren, *Eur. J. Inorg. Chem.*, 2004, **2004**, 2232.
82 A. C. Tsipis, *Organometallics*, 2012, **31**, 7206.
83 A. C. Tsipis and A. V. Stalikas, *Inorg. Chem.*, 2012, **51**, 2541.
84 A. C. Tsipis and D. N. Gkarmpounis, *J. Comput. Chem.*, 2012, **33**, 2318.
85 J. Baldenebro-Lopez, N. Flores-Holguin, J. Castorena-Gonzalez, J. Almaral-Sanchez and D. Glossman-Mitnik, *Int. J. Photoenergy*, 2013, **2013**, 1.
86 Y. Chen and S. Sakaki, *Inorg. Chem.*, 2013, **52**, 13146.
87 M. Pavelka and J. V. Burda, *Chem. Phys.*, 2005, **312**, 193.
88 A. C. Tsipis and P. A. Karipidis, *Polyhedron*, 2008, **27**, 289.
89 T. Afrati, C. Dendrinou-Samara, C. Raptopoulou, A. Terzis, V. Tangoulis, A. Tsipis and D. P. Kessissoglou, *Inorg. Chem.*, 2008, **47**, 7545.
90 V. S. Bryantsev, M. S. Diallo, A. C. T. van Duin and W. A. Goddard III, *J. Phys. Chem. A*, 2008, **112**, 9104.
91 V. S. Bryantsev, M. S. Diallo and W. A. Goddard III, *J. Phys. Chem. A*, 2009, **113**, 9559.
92 A. Ghosh, T. Wondimagegn and A. B. J. Parusel, *J. Am. Chem. Soc.*, 2000, **122**, 5100.
93 J. Hu, Q. Chen, H. Hu, Z. Jiang, D. Wang, S. Wang and Y. Li, *J. Phys. Chem. A*, 2013, **117**, 12280.
94 M. Bröring, F. Brégier, E. Cónsul Tejero, C. Hell and M. C. Holthausen, *Angew. Chem., Int. Ed.*, 2007, **46**, 445.
95 A. B. Alemayehu, E. Gonzalez, L. K. Hansen and A. Ghosh, *Inorg. Chem.*, 2009, **48**, 7794.
96 K. Pierloot, H. Zhao and S. Vancoillie, *Inorg. Chem.*, 2010, **49**, 10316.
97 T. Miteva, J. Romanova, A. Ivanova, A. Tadjer and M. Baumgarten, *Eur. J. Inorg. Chem.*, 2010, **2010**, 379.
98 C. Wang, X. Zhang, Q.-S. Li, Y. Xie, R. B. King and H. F. Schaefer III, *J. Mol. Model.*, 2012. **18**, 2387.
99 H. C. Kolb, M. G. Finn and K. B. Sharpless, *Angew. Chem., Int. Ed.*, 2001, **40**, 2004.
100 R. Berg and B. F. Straub, *Beilstein J. Org. Chem.* 2013**, 9**, 2715.
101 R.Huisgen, *Angew. Chem.*, 1963, **75**, 604.
102 F. Himo, T. Lovell, R. Hilgraf, V. V. Rostovtsev, L. Noodleman, K. B. Sharpless and V. V. Fokin, *J. Am. Chem. Soc.*, 2005, **127**, 210.
103 B. F. Straub, *Chem. Commun.*, 2007, 3868.
104 D. Cantillo, M. Ávalos, R. Babiano, P. Cintas, J. L. Jiménez and J. C. Palacios, *Org. Biomol. Chem.*, 2011, **9**, 2952.
105 S. Calvo-Losada, M. S. Pino and J. J. Quirante, *J. Mol. Model.*, 2014, **20**, 2187.

106 A. Reichelt and S. F. Martin, *Acc. Chem. Res.*, 2006**,** **39**, 433.
107 J. Salaun and M. S. Baird, *Curr. Med. Chem.*, 1995**,** **2**, 511.
108 B. F. Straub, I. Gruber, F. Rominger and P. Hofmann, *J. Organomet. Chem.* 2003**,** **684**, 124.
109 J. M. Fraile, J. I. García, V. Martínez-Merino, J. A. Mayoral and L. Salvatella, *J. Am. Chem. Soc*., 2001, **123**, 7616.
110 B. F. Straub, I. Gruber, F. Rominger and P. Hofmann, *J. Organomet. Chem.*, 2003, **684**, 124.
111 G. Drudis-Solé, F. Maseras, A. Lledós, A. Vallribera and M. Moreno-Mañas, *Eur. J. Org. Chem.* 2008, **2008**, 5614.
112 J. I. García, G. Jiménez-Osés and J. A. Mayoral, *Chem. Eur. J*., 2011, **17**, 529.
113 S. Aguado-Ullate, M. Urbano-Cuadrado, I. Villalba, E. Pires, J. I. García, C. Bo and J. J. Carbó, *Chem. Eur. J.*, 2012, **18**, 14026.
114 F. Ullmann, *Ber. Dtsch. Chem. Ges.*, 1903, **36**, 2382.
115 F. Ullmann, *Ber. Dtsch. Chem. Ges.*, 1904, **37**, 853.
116 I. Goldberg, *Ber. Dtsch. Chem. Ges*., 1906, **39**, 1691.
117 E. Sperotto, G. P. M. van Klink, G. van Koten and J. G. de Vries, *Dalton Trans.*, 2010, **39**, 10338.
118 S.-L. Zhang , L. Liu , Y. Fu and Q.-X. Guo, *Organometallics*, 2007, **26**, 4546.
119 C.-H. Guo, H.-S. Wu, X.-M. Zhang, J.-Y. Song and X. Zhang, *J. Phys. Chem. A* 2009, **113**, 6710.
120 G. O. Jones, P. Liu, K. N. Houk and S. L. Buchwald, *J. Am. Chem. Soc.*, 2010, **132**, 6205.
121 S. Ranjit, R. Lee, D. Heryadi, C. Shen, JE Wu, P. Zhang, K.-W. Huang and X. Liu, *J. Org. Chem.*, 2011, **76**, 8999.
122 L. Sikk, J. Tammiku-Taul, P. Burk and A. Kotschy, *J. Mol. Model*., 2012, **18**, 3025.
123 C. Zhang, C. Tanga and N. Jiao, *Chem. Soc. Rev*., 2012, **41**, 3464.
124 G.-J. Cheng, L.-J. Song, Y.-F. Yang, X. Zhang, O. Wiest and Y.-D. Wu, *ChemPlusChem*, 2013, **78**, 943.
125 L.-H. Zou, A. J. Johansson, E. Zuidema and C. Bolm, *Chem. Eur. J*., 2013, **19**, 8144.
126 Q. Wang, J.-F. Jia, C.-H. Guo and H.-S. Wu, *J. Organomet. Chem.*, 2013, **748**, 84.
127 G. Jiménez-Osés, E. Vispe, M. Roldán, S. Rodríguez-Rodríguez, P. López-Ram-de-Viu, L. Salvatella, J. A. Mayoral and J. M. Fraile, *J. Org. Chem.*, 2013, **78**, 5851.
128 S. Rendler and M. Oestreich, *Angew. Chem. Int. Ed.*, 2007, **46**, 498.
129 H. Brunner and W. Miehling, *J. Organomet. Chem.*, 1984, **275**, C17.
130 T. Gathy, D. Peeters and T. Leyssens, J. Organomet. Chem., 2009, **694**, 3943.
131 J.-T. Issenhuth, F.-P. Notter, S. Dagorne, A. Dedieu and S. Bellemin-Laponnaz, *Eur. J. Inorg. Chem.*, 2010, **2010**, 529.
132 T. Vergote, T. Gathy, F. Nahra, O. Riant, D. Peeters and T. Leyssens, *Theor. Chem. Acc.*, 2012, **131**, 1253.
133 T. Vergote, F. Nahra, D. Peeters, O. Riant and T. Leyssens, *J. Organomet. Chem.*, 2013, **730**, 95.
134 Y. Zhao, Y. Liu, S. Bi and Y. Liu, *J. Organomet. Chem.*, 2013, **745-746**, 166.
135 P. Gamez, P. G. Aubel, W. L. Driessen and J. Reedijk, *Chem. Soc. Rev.*, 2001, **30**, 376.
136 J. I. van der Vlugt and F. Meyer, *Top. Organomet. Chem.*, 2007, **22**, 191.
137 A. E. Wendlandt, A. M. Suess and S. S. Stahl, *Angew. Chem. Int. Ed.*, 2011, **50**, 11062.
138 A. E. King, L. M. Huffman, A. Casitas, M. Costas ‡, X. Ribas and S. S. Stahl, *J. Am. Chem. Soc*., 2010, **132**, 12068.
139 X. Ribas, C. Calle, A. Poater, A. Casitas, L. Gómez, R. Xifra, T. Parella, J. Benet-Buchholz, A. Schweiger, G. Mitrikas, M. Solà, A. Llobet and T. D. P. Stack, *J. Am. Chem. Soc.*, 2010, **132**, pp 12299.
140 A. Poater, X. Ribas, A. Llobet, L. Cavallo and M. Solà, *J. Am. Chem. Soc.*, 2008, **130**, 17710.
141 T. Kamachi, Y.-M. Lee, T. Nishimi, J. Cho, K. Yoshizawa and W. Nam, *J. Phys. Chem. A*, 2008, **112**, 13102.
142 S. M. Hubera, M. Z. Ertema, F. Aquilante, L. Gagliardia, W. B. Tolmana and C. J. Cramer, *Chemistry*, 2009; **15**, 4886.
143 M. Güell, J. M. Luis, M Solá, and P. E. M. Siegbahn, *J. Biol. Inorg. Chem.*, 2009, **14**, 229.
144 M. C. Paderes, L. Belding, B. Fanovic, T. Dudding, J. B. Keister and S. R. Chemler, *Chem. Eur. J*., 2012, **18**, 1711.
145 L. Belding, S. R. Chemler and T. Dudding, *J. Org. Chem.*, 2013, **78**, 10288.
146 P. E. M. Siegbahn and M. Wirstam, *J. Am. Chem. Soc*., 2001, **123**, 11819.
147 R. Prabhakar and P. E. M. Siegbahn, *J. Phys. Chem. B*, 2003, **107**, 3944.

148 M. Pavelka, M. Šimánek, J.´ Šponer and J. V. Burda, *J. Phys. Chem. A*, 2006, **110**, 4795.
149 M. Pavelka and J. V. Burda, *Mol. Phys.*, 2008, 106, 2733.
150 T. Suksrichavalit, S. Prachayasittikul, T. Piacham, C. Isarankura-Na-Ayudhya, C. Nantasenamat and V. Prachayasittikul, *Molecules* 2008, **13**, 3040.
151 P. de Hoog, M. J. Louwerse, P. Gamez, M. Pitié, E. J. Baerends, B. Meunier and J. Reedijk, *Eur. J. Inorg. Chem.* 2008, **2008**, 612.
152 J. C. Garíca-Ramos, A. Tovar-Tovar, J. Hernández-Lima, F. Cortés-Guzmán, R. Moreno-Esparza and L. Ruiz-Azuara, *Polyhedron*, 2011, **30**, 2697.
153 R. Galindo-Murillo, J. Hernandez-Lima, M. Gonzalez-Rendon, F. Cortés-Guzmán, L. Ruiz-Azuara and R. Moreno-Esparza, *Phys. Chem. Chem. Phys.*, 2011, **13**, 14510.
154 R Galindo-Murillo, L. Ruíz-Azuara, R. Moreno-Esparzac and F. Cortés-Guzmá, *Phys. Chem. Chem. Phys.*, 2012, **14**, 15539.
155 E. I. Solomon and R. G. Hadt, *Coord. Chem. Rev.*, 2011, **255**, 774.
156 A. Kunishita, M. Z. Ertem, Y. Okubo, T. Tano, H. Sugimoto, K. Ohkubo, N. Fujieda, S. Fukuzumi, C. J. Cramer and Shinobu Itoh, *Inorg. Chem.*, 2012, **51**, 9465.
157 M. Bruschi, L. Bertini, V. Bonačić-Koutecký,‡ L. De Gioia,† R. Mitrić, G. Zampella and P. Fantucci, *J. Phys. Chem. B*, 2012, **116**, 6250.
158 A. Miličević and N. Raos, Arh. Hig. Rada. Toksikol., 2013;**64**, 539.
159 A. Rimola, J. Alí-Torres, C. Rodríguez-Rodríguez, J. Poater, E. Matito, M. Solà and M. Sodupe, *J. Phys. Chem. A*, 2011, **115**, 12659.
160 L. Quintanar, L. Rivillas-Acevedo, R. Grande-Aztatzi, C. Z. Gómez-Castro, T. Arcos-López and A. Vela, *Coord. Chem. Rev.*, 2013, **257**, 429.
161 N. M. Aburas, N. R. Stevanović, M. K. Milčić, A. Đ. Lolić, M. M. Natić, Ž. Lj. Tešić and R. M. Baošić, *J. Braz. Chem. Soc.*, 2013, **24**, 1322.
162 S. Blasco, M. I. Burguete, M. Paz Clares, E. García-España, J. Escorihuela and S. V. Luis, *Inorg. Chem.* 2010, **49**, 7841.
163 S. Blasco, Begoña Verdejo, M. Paz Clares, C. E. Castillo, A. G. Algarra, J. Latorre, M. A. Máñez, M. G. Basallote, C. Soriano and E. García-España, *Inorg. Chem.* 2010, **49**, 7016.
164 C. E. Castillo, J. González-García, J. M. Llinares, M. A. Máñez, H. R. Jimenez, E. García-España and M. G. Basallote, *Dalton Trans.*, 2013, **42**, 6131.
165 I. Martí, A. Ferrer, J. Escorihuela, M. I. Burguete and S. V. Luis, *Dalton Trans.*, 2012, **41**, 6764.
166 D. Jacquemin, B. Mennucci and C. Adamo, *Phys. Chem. Chem. Phys.*, 2011, **13**, 16987.
167 A.D. Laurent and D. Jacquemin, *Int. J. Quantum Chem.* 2013, **113**, 2019.
168 C. Garino and L. Salassa, *Phil. Trans. R. Soc. A* 2013, **371**, 20120134 and references therein.
169 N. Armaroli, G. Accorsi, F. Cardinali and A. Listorti, *Top. Curr. Chem.*, 2007, **280**, 69.
170 L. X. Chen, G. B. Shaw, I. Novozhilova, T. Liu, G. Jennings, K. Attenkofer, G. J. Meyer and P. Coppens, *J. Am. Chem. Soc.*, 2003, **125**, 7022.
171 Z. A. Siddique, Y. Yamamoto, T. Ohno and K. Nozaki, *Inorg. Chem.*, 2003, **42**, 6366.
172 X. Wang, W. Wang, M. Koyamac, M. Kubo and A. Miyamotoc, *J. Photochem. Photobiol. A: Chemistry*, 2006, **179**, 149.
173 W. H. Lam, E. C.-C. Cheng and V. W.-W. Yam, *Inorg. Chem.*, 2006, **45**, 9434.
174 A. Lavie-Cambot, M. Cantuela, Y. Leydet, G. Jonusauskas, D. M. Bassania and N. D. McClenaghan, *Coord. Chem. Rev.*, 2008, **252**, 2572.
175 B. Hu, G. Gahungu and J. Zhang, *J. Phys. Chem. A*, 2007, **111**, 4965.
176 P. Aslanidis, P. J. Cox, K. Kapetangiannis and A. C. Tsipis, *Eur. J. Inorg. Chem.*, 2008, **2008**, 5029.
177 J. P. Holland and J. C. Green, J. Comput. Chem., 2010, 31: 1008.
178 P. Aslanidis, P. J. Cox and A. C. Tsipis, *Dalton Trans.*, 2010, **39**, 10238.
179 A. Alemayehu, J. Conradie and A. Ghosh, *Eur. J. Inorg. Chem.*, 2011, **2011**, 1857.
180 K. J. de Almeida, T. C. Ramalho. Z. Rinkevicius, O. Vahtras, H. Ågren, and A. Cesar, *J. Phys. Chem. A*, 2011, **115**, 1331.
181 L.-Y. Zou, M.-S. Maa, Z.-L. Zhang, H. Li, Y.-X. Cheng and A.-M. Ren, *Organic Electronics*, 2012, **13**, 2627.
182 M. Kayanuma, N. Bera, M. Sandroni, Y. Pellegrin, E. Blart, F. Odobel and C. Daniel, *C. R. Chimie*, 2012, **15**, 255.
183 M. Rohrmüller, S. Herres-Pawlis, M. Witte and W. G. Schmidt, *J. Comput. Chem.*, 2013, **34**, 1035.

184 M. J. Leitl, F.-R. Küchle, H. A. Mayer, L. Wesemann and H. Yersin, *J. Phys. Chem. A*, 2013, **117**, 11823.
185 J. Baldenebro-Lopeza, N. Flores-Holguina, J. Castorena-Gonzalez and D. Glossman-Mitnika, *J. Photochem. Photobiol. A: Chemistry*, 2013, **267**, 1.
186 J.-L. Chen, X.-F. Cao, J.-Y. Wang, Li.-H. He, Z.-Y. Liu, H.-R. Wen and Z.-N. Chen, *Inorg. Chem.*, 2013, **52**, 9727.
187 H. R. Zhekova, M. Seth and T. Ziegler, *Int. J. Quant. Chem.*, 2014, DOI: 10.1002/qua.24624.
188 C. Saracini, D. G. Liakos, J. E. Zapata Rivera, F. Neese, G. J. Meyer and K. D. Karlin, *J. Am. Chem. Soc.*, 2014, **136**, 1260.